

**FUNCTIONAL MORPHING FOR MANUFACTURING PROCESS
DESIGN, EVALUATION AND CONTROL**

by

Liang Zhou

A dissertation submitted in partial fulfillment
of the requirements for the degree of
Doctor of Philosophy
(Mechanical Engineering)
in The University of Michigan
2010

Doctoral Committee:

Professor Shixin Jack Hu, Chair

Professor Gregory M. Hulbert

Associate Professor Jionghua Jin

Thomas B. Stoughton, General Motors

Liang Zhou

©

All Rights Reserved

2010

ACKNOWLEDGMENTS

I would like to thank my advisor, committee members, colleagues, friends, and family for their help and support. Without them, I would never have been able to finish this dissertation.

Sincere gratitude goes to my advisor and chair Professor S. Jack Hu for his continuous encouragement and help through my Ph.D. studies. His vast knowledge, vision and support were fortunes to me during the past 5 years. Professor Hu taught me how to think critically, and to write and express myself clearly.

I would also like to extend gratitude to my other committee members, Professor Jionghua Jin, Professor Gregory M. Hulbert and Dr. Thomas B. Stoughton for their constructive suggestions and valuable discussion while in pursuit of my studies. I especially appreciate Dr. Stoughton's vision and support through the discussions of my research.

I am also grateful to Dr. Pei-Chung Wang, who opened the door of automotive manufacturing for me and gave me tremendous help in both research and life. My interaction with Dr. Wang benefited me both professionally and personally.

I also want to express my acknowledgment to General Motors Corporation for the financial and technical support of my research, especially Dr. Susan Smyth, Dr. Jeff Abel and Dr. Roland Menassa who have always offered their constructive support. In

remembrance, I would also like to thank Dr. Samuel P. Marin whose insight and kindness have set a goal I wish to achieve in my life time. I also want to express my thank to Dr. Raymond Sarraga, Dr. Wayne Cai, Dr. Chih-Cheng Hsu, Daniel Hayden, John Fickes, Steve Koshorek, Dr. Wu Yang and all the colleagues I have worked with for their support and help throughout these years.

Special thanks to Dr. Guosong Lin and Dr. Hui Wang who have worked with me closely on my research. They offered me much help and encouragement to overcome technical obstacles I have faced. I am deeply indebted to them.

My gratitude also goes to my friends and colleagues in Hu-Lab, Dr. Tae Kim, John Wang, Jingjing Li, Sha Li, Xiaoning Jin, Shawn Lee, Hai Trong Nguyen, Saumuy Suriano, Chenhui Shao, Robert Riggs, Taylor Tappe, Vernnaliz Carrasquillo, and former colleagues Dr. Yuanyuan Zhou, Dr. Xiaowei Zhu, Dr. Jian Liu, Dr. April Bryan, Dr. Luis Eduardo Izquierdo, Dr. Hao Du, Dr. Ugur Ersoy, Dr. Joenghan Ko and Dr. Jianpeng Yue for providing a stimulating and open environment for thinking and research. Special thank also goes to Constance Raymond-Schenk and Kathy Brochner for their continuous administrative help and support.

Most importantly, none of these would have been possible without the love and support from my family. I want to express my greatest appreciation to my parents for their faith in me and unconditional love, concern and support. I also owe gratitude to my fiancé, Xiaohong Zhang, for the love, support and happiness she has brought to my life.

I owe my gratitude to all those people who have made this dissertation possible and made my doctoral study experience possible.

TABLE OF CONTENTS

ACKNOWLEDGMENTS	ii
LIST OF FIGURES	vii
LIST OF TABLES.....	xi
ABSTRACT	xii
CHAPTER 1 INTRODUCTION.....	1
1.1. Motivation.....	1
1.2. Literature Review.....	5
1.2.1. Image Transformation	5
1.2.2. Morphing in Process Design, Evaluation and Control	6
1.2.3. Summary of Literature Review	10
1.3. Research Objectives.....	10
1.4. Organization of Dissertation	11
References.....	13
CHAPTER 2 FUNCTIONAL MORPHING BASED EVOLUTIONARY STAMPING DIE DEVELOPMENT	19
2.1. Introduction.....	20
2.2. Die Face Morphing Algorithm.....	22
2.2.1. Free-Form Representation for Part and Die	24
2.2.2. Part-to-Part Mapping by FFD Based Transformation	25
2.2.3. Die-to-Die Morphing.....	31
2.2.4. Consideration on Trimmed Surfaces.....	31
2.3. Case Study	33
2.3.1. 2D Study on Stamping U-shaped Channel.....	33
2.3.2. 3D Case Study on Cup Drawing	36

2.3.3. Mapping of Trimmed Surface	39
2.4. Conclusion	42
References.....	42

**CHAPTER 3 FUNCTIONAL MORPHING BASED FORMABILITY
ASSESSMENT IN STAMPING DIE FACE MORPHING USING
STRAIN INCREMENT METHOD.....44**

3.1. Introduction.....	45
3.2. State-Of-The-Art.....	46
3.3. The Strain Increment Method	48
3.3.1. Geometric Mapping by Free-Form Deformation	48
3.3.2. Overview of the Strain Increment Method.....	49
3.3.3. Mapping of FE Mesh to Geometry.....	50
3.3.4. Strain Increment from Displacement	52
3.3.5. Bending Energy and Strain Gradient Functions.....	55
3.4. Case Study	58
3.4.1. 2D U-shaped Channel Stamping	58
3.4.2. Generation of New Die Surface	59
3.4.3. Strain Prediction by Strain Increment Method.....	60
3.4.4. 3D Case Study on Cup Drawing	61
3.5. Conclusion	64
References.....	65

**CHAPTER 4 FUNCTIONAL MORPHING IN MULTI-STAGE
MANUFACTURING AND ITS APPLICATIONS IN
HIGH-DEFINITION METROLOGY BASED PROCESS
CONTROL.....68**

4.1. Introduction.....	69
4.2. Modeling of Surface Changes Using Functional Morphing	72
4.2.1. Feature Extraction	73
4.2.2. Functional Morphing for Surfaces	74

4.2.3. Morphing Based Multi-stage Variation Modeling	79
4.3. Applications of Functional Morphing in Machining Process Control....	82
4.3.1. Inter-stage Process Adjustment	82
4.3.2. Backward Morphing Based Process Monitoring.....	84
4.3.3. Process Tolerance Design	85
4.4. Case Study	86
4.4.1. Experimental Setup	86
4.4.2. Functional Morphing Between Stages	88
4.4.3. Inter-stage Process Adjustment	89
4.4.4. Backward Morphing Based Process Monitoring.....	93
4.5. Conclusion	95
References.....	97

CHAPTER 5 CONCLUSIONS AND FUTURE WORK.....100

5.1. Conclusions.....	100
5.2. Future Work	104

LIST OF FIGURES

Figure 1.1	Example of morphing [Lee, et al. 1996].....	2
Figure 1.2	Feature based on product design [Hsiao and Liu, 2002]	2
Figure 1.3	Surface feature morphing	4
Figure 1.4	Research framework.....	12
Figure 2.1	Product family of Chevy Malibu from 1997 to 2008.....	20
Figure 2.2	Mapping from old generation to new generation	21
Figure 2.3	Die face morphing concept.....	24
Figure 2.4	NURBS surface defined by 16 (4×4) control points	25
Figure 2.5	Free form deformation: (x,y,z) is the original point, (X,Y,Z) is the new point after FFD.....	27
Figure 2.6	Comparison with and without including smoothing function	29
Figure 2.7	Sample of trimmed surface.....	32
Figure 2.8	Boundary lines of sample trimmed surface	32
Figure 2.9	(A) original die; (B) original part after springback; (C) desired new part with a concave feature at bottom (after springback).....	34
Figure 2.10	Part-to-part mapping (dots: lattice points, cross: control points of	

morphed original part, circle: desired new part, line: NURBS curve generated from the control points).....	35
Figure 2.11 Die-to-die morphing (dots: lattice points, Cross: control points of the morphed die, solid line: Die surface, dashed line: desired part surface)	35
Figure 2.12 Comparison of the part generated from the morphed die (solid line) to the desired part (circled line)	36
Figure 2.13 3D cup drawing case study: (A) shape of the existing part; (B) shape of the new part; (C) 1/8 modeling. (x: NURBS control points of the existing part, o: NURBS control points of the new part).....	37
Figure 2.14 Part-to-part mapping of 3D cup drawing.....	38
Figure 2.15 The new die face generated from the evolutionary die morphing method	38
Figure 2.16 Comparison of the part generated by the morphed die (point cloud) and the desired part (surface).....	39
Figure 2.17 Case study of trimmed surfaces mapping.....	40
Figure 2.18 Part-to-part mapping for trimmed surfaces	40
Figure 2.19 Boundary groups by K-Means.....	41
Figure 2.20 Die face morphing for trimmed surface	41
Figure 3.1 Mapping of finite element nodes (dots) on to geometry (crosses are B-spline control points).....	51
Figure 3.2 Strain prediction in 2D by “length of the line”	53

Figure 3.3	Lamina coordinate and fiber direction in a shell element [Hughes, 2000]	53
Figure 3.4	2D U-shaped channel case study: (A) existing die and boundary conditions; (B) shape of the existing part; (C) shape of the new part....	59
Figure 3.5	Mapping of finite element mesh onto geometry.....	59
Figure 3.6	Part-to-part mapping solved from (3.13).....	59
Figure 3.7	Strain prediction on the existing and new parts by FEA	60
Figure 3.8	Strain increment.....	61
Figure 3.9	Strain prediction by FEA and strain increment method	61
Figure 3.10	Strain prediction on the existing and new parts by FEA	62
Figure 3.11	Strains from edge to center of the new part.....	63
Figure 4.1	V-8 engine head measured by HDM device	69
Figure 4.2	Projection of scattered data onto grids	74
Figure 4.3	Schematic diagram for multi-stage process monitoring.....	84
Figure 4.4	Experimental setup	87
Figure 4.5	Feature extraction for global shape deformation.....	89
Figure 4.6	Functional morphing for 2-stage manufacturing process.....	89
Figure 4.7	Finite element analysis of face milling process (displacement in Z)	90
Figure 4.8	Finite element analysis of drilling process (displacement in Z).....	91
Figure 4.9	Case study on inter-stage form error compensation	93

Figure 4.10 Scree plot of 100 training data.....	94
Figure 4.11 Phase I Hotelling's T^2 control chart at final stage	94
Figure 4.12 Phase I Hotelling's T^2 control chart at prior stages	94
Figure 4.13 Phase II control charts	95

LIST OF TABLES

Table 2.1 Material properties of AA6111-T4.....	36
Table 3.1 Element connectivity matrix	52
Table 4.1 Comparison of Free-Form Deformation and Thin Plate Spline.....	75
Table 4.2 Manufacturing system for inter-stage error compensation	83
Table 4.3 Mechanical properties of Aluminum Alloy 2024.....	87
Table 4.4 Variance sources in face milling stage	90
Table 4.5 Variance sources in drilling stage.....	91
Table 4.6 Adjustable process parameters and optimal values.....	92
Table 4.7 Comparison of surface flatness with and without compensation.....	93

ABSTRACT

Shape changes are commonly identified in product development and manufacturing. These changes include part shape changes in a product family from one generation to another, surface geometric changes due to manufacturing operations, etc. *Morphing* is one method to mathematically model these shape changes. However, conventional morphing focuses only on geometric change without consideration of process mechanics/physics. It thus has limitations in representing a complex physical process involved in product development and manufacturing. This dissertation proposes a *functional morphing* methodology which integrates physical properties and feasibilities into geometric morphing to describe complex manufacturing processes and applies it to manufacturing process design, evaluation, and control.

Three research topics are conducted in this dissertation in areas of manufacturing process design, evaluation and control. These are:

- *Development of evolutionary stamping die face morphing*: Similarities which are identified among parts of the same product family allow the possibilities for the knowledge learned from the die design of one generation of sheet metal product to be morphed onto that of a new but similar product. A new concept for evolutionary die design is proposed using a functional morphing algorithm. Case studies show that the proposed method is able to capture the added features in the new part design as well as the springback compensation inherited from the existing die face.
- *Formability assessment in die face morphing*: A strain increment method is proposed for early formability assessment by predicting strain

distribution directly from the part-to-part mapping process based on the functional morphing algorithm. Since this method does not require the knowledge on the new die surface, such formability assessment can serve as an early manufacturing feasibility analysis on the new part design.

- *Functional morphing in monitoring and control of multi-stage manufacturing processes:* A functional free form deformation (FFD) approach is developed to extract mapping functions between manufacturing stages. The obtained mapping functions enable multi-scale variation propagation analysis and intermediate-stage process monitoring. It also allows for accurate inter-stage adjustment that introduces shape deformation upstream to compensate for the errors downstream.

CHAPTER 1

INTRODUCTION

1.1. MOTIVATION

Geometry or shape change exists everywhere in our daily life. The changes in an object's location are described using words such as “translate”, “rotate”, “shift”, etc., while the changes in an object's shape are described using “deform”, “bend”, “elongate”, etc. In computer graphics, the amount of change is quantitatively measured by *image transformation* utilizing mathematical methods, in which rigid transformation is used to characterize the change of location and non-rigid transformation is used to describe the change of the object itself.

Morphing is one image transformation method describing a complex and seamless transition of an object from one shape to another. It is widely used in the areas of computer graphics, filming, medical imaging, etc. In computer graphics and filming, morphing is an animation technique by which one graphic object is gradually turned into another using methods such as cross-dissolve, warping, interpolation, etc. Figure 1.1 is an example of face morphing using cross-dissolve which combines the first and last images with weights. Morphing is also used for video encoding and compression, where static scenes are connected by morph models [Shum, et al. 2003; Galpin, et al. 2004]. Morphing algorithms are developed and utilized in medical imaging where

images taken from Computed Tomography (CT) and/or Magnetic Resonance Imaging (MRI) are aligned (registered) by morphing methods to minimize their variance for better disease diagnosis [Rueckert, et al. 1999; Wang, et al. 2007].



Figure 1.1 Example of morphing [Lee, et al. 1996]

In product design and engineering, morphing algorithms have been adopted for product shape design in which feature based design [Hsiao and Liu, 2002] and parametric design [Roth, et al. 2002; Roth and Crossley, 2003] are conducted. Reverse engineering [Piegl, et al. 2001; Li and Ni, 2009] makes use of morphing to regenerate parametric surfaces based on measured point clouds. Morphing in these areas is mostly data driven and appearance/feature oriented. For example, new design of a LCD monitor in Figure 1.2 is morphed from previous designs with minor feature changes.

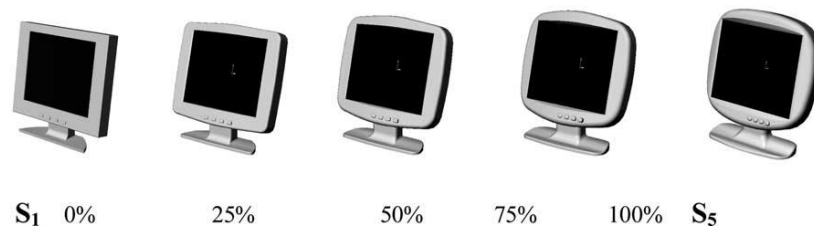


Figure 1.2 Feature based on product design [Hsiao and Liu, 2002]

Shape change is an important goal of most manufacturing processes, which could be described by morphing. However, very limited research exists in applying morphing to manufacturing, including process design, evaluation and control. Morphing can help facilitate process design in which process knowledge and similarities from previous product generations can be inherited for new process design of a new generation

product. For example, in sheet metal stamping die development, previous generation dies can be morphed into new dies where the knowledge of formability can be quickly learned in the new die before die design completion. Morphing can also be used in process control to characterize the shape change from one stage to another, therefore, making it feasible to monitor the intermediate stages based on end-of-line measurement. In addition, the shape characteristics from the intermediate stages provide opportunities for compensation of the end-of-line form errors.

However, conventional morphing used in filming, design, etc. only describes the geometry/shape changes between graphic objects without consideration of material and physical properties and processes. In manufacturing, morphing effect should characterize the changes of physical objects associated with mechanical properties and processes in addition to the changes in geometry and shape. For instance, Figure 1.3 describes the part top surface changes from two operations: milling and drilling. It can be seen from Figure 1.3(C, D) that surface exiting drilling operation differs from milling operation in both global shape and local defect (a small bump in the middle). Such changes are the result of the joint effect of the geometrical shape due to the cutter path and the mechanical/materials interactions of cutting force, deformation and springback.

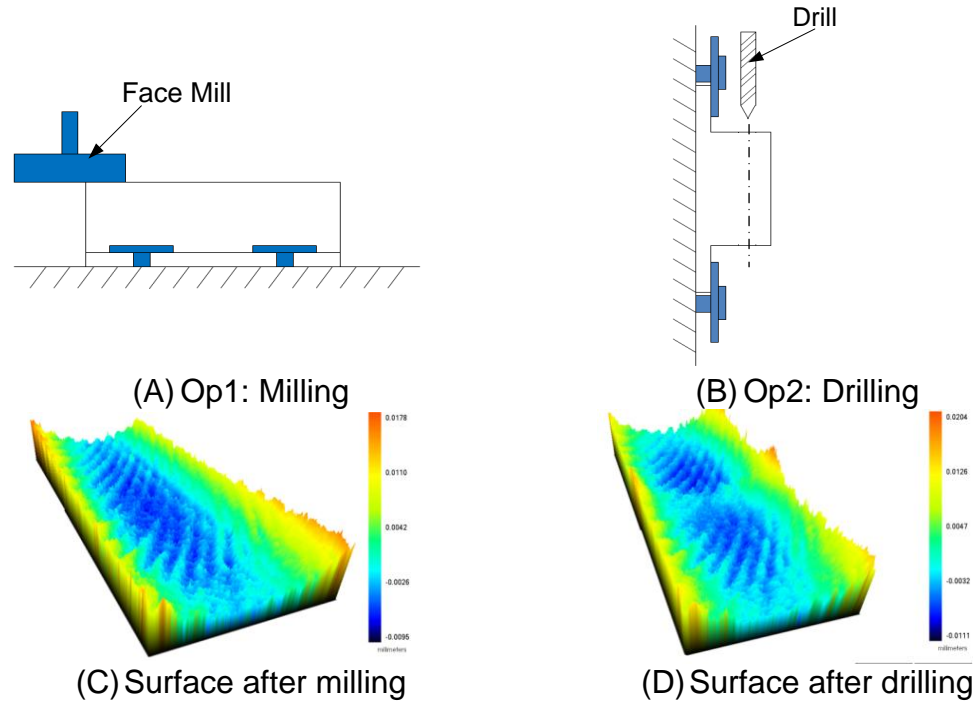


Figure 1.3 Surface feature morphing

This dissertation develops “*functional morphing*”, a methodology to describe the geometric shape changes by incorporating physical feasibility in terms of mechanical properties, process conditions, etc., instead of using pure geometries alone. Using functional morphing, shape changes can be better interpreted based on physical properties and/or process conditions. Functional morphing can further facilitate process design, evaluation and control incorporating the knowledge of process information in addition to geometric morphing. For example, stamping dies can be designed using functional morphing from prior generations to the current generation by integrating springback compensation. Formability can be evaluated by morphing one part to another while satisfying physical feasibility (i.e., equilibrium state). Furthermore, functional morphing can be used in a multi-stage manufacturing system to relate the product shape changes to stage operations (e.g., machining, drilling and milling) for quality improvement. This thesis develops functional morphing algorithms

and explores the applications in manufacturing process design, evaluation and control.

1.2. LITERATURE REVIEW

This section conducts a comprehensive review of related literature on morphing and the research attempts using morphing in manufacturing process development and control.

1.2.1. Image Transformation

In computer graphics, morphing effects are captured by mathematical transformation which maps any point on the source object to the corresponding point on the target object. The most commonly used transformation techniques include affine transformation and quadratic transformation [Hearn and Baker, 1994], and free-form deformation (FFD) [Sederberg and Parry, 1986; Coquillart, 1990]. The affine transformation is usually utilized for rigid body but lacks the degrees of freedom needed to describe the complex shape changes. Quadratic transformation offers more but still limited degrees of freedom. FFD are commonly adopted for more complex shape changes with localized deformation. However, these image transformation methods and applications are mostly data-oriented and may yield transformations that are difficult to be interpreted since no physical insights are provided.

Researches were attempted in integrating mechanical attributes into conventional morphing algorithm. Thin-Plate Spline (TPS) [Bookstein, 1989], which is derived from minimization of bending energy of a thin plate subjected to key points constraints, is one such effort. Radial basis functions are introduced to interpolate the intermediate points besides those key points. In medical imaging research, smoothness function is

also integrated into image transformation [Rueckert, et al. 1999; Hill, et al. 2001] so that a smooth transformation concerning continuity is satisfied. In manufacturing, such smoothness is not sufficient to accurately characterize the change of shape, for example, of a non-homogenous density distribution or heterogeneous material. Therefore, functional morphing in manufacturing will need a more accurate measure of physical attributes.

1.2.2. Morphing in Process Design, Evaluation and Control

Manufacturing Process Design

Manufacturing process design often involves process selection, process parameter design, and tooling/fixture design. Process selection and parameter design are performed by examining the shape and tolerance requirements of individual features, selecting a process that is capable of meeting the requirements and choosing the process parameters so as to minimize the effects on performance arising from variation in manufacture, environment and cumulative damage. This line of research includes robust parameter design by Feng and Kusiak [1996, 1997, 2000], loss function based tolerance allocation by Anwarul and Liu [1995], Choi et al. [2000], and Li [2000, 2002], economic design by Jeang [2002] and multistage process tolerance design [Huang and Shi, 2003; Ding, et al. 2005]. Efforts have also been made by researchers to address several parameter issues at the same time. For example, Jeang and Chang [2002] proposed to concurrently optimize process mean and tolerances. Zhang [1997] developed simultaneous tolerance analysis and synthesis; Huang and Shi [2003] developed simultaneous tolerance synthesis via variation propagation modeling. Among these studies, design of experiment (DOE), response surface model and

Taguchi's robust parameter design are commonly used methodologies.

In tooling and fixture design, efforts were made to improve the key product characteristics (KPC) by optimizing choice of fixture and location schemes. Cai et al. [1997] proposed a variational method for robust fixture configuration design for 3D rigid parts. Wang and Pelinescu [2001] developed an algorithm for fixture synthesis of 3D workpieces by selecting the positions of the clamps from a collection of locations. In the design of fixtures for compliant parts, finite element method is used to model and analyze workpiece behavior [Lee and Haynes, 1987]. Camelio et al. [2004] determined the optimal fixture location to hold sheet metal parts considering out of plane variation of fixtures. Cai and Hu [1996] studied the use of the "N-2-1" fixture to provide additional support for the part and reduce the part's deformation. Izquierdo et al. [2009] introduced robust fixture layout design for multistage manufacturing lines.

Morphing in design area mostly focuses on product design involving appearance or shape evolutions. Research in product design using morphing can be found in [Hsiao and Liu, 2002; Roth and Crossley, 2002; Roth, et al. 2003]. In process design, morphing algorithms have recently been developed to facilitate CAD/CAE processes. Mesh morphing is integrated into some commercial software such as *DynaForm* and *HyperMesh* to improve development efficiency by quickly changing the finite element mesh from one product to another. It is also used for multi-objective process optimization [Liu and Yang, 2007]. Morphing is utilized in stamping die design to iteratively compensate springback given the simulated springback information [Yin, 2004; Sarraga, 2004].

Process Evaluation

There are two major research topics on process evaluation: (1) manufacturability evaluation to determine whether the designed process is capable of producing the product, (2) process capability and sensitivity analysis to achieve high repeatability and low variability. Traditionally, process evaluation followed an experience-based and trial-and-error procedure. With the introduction of computer graphics and CAD/CAM systems, numerical approaches have been widely adopted in process evaluation. Finite element method (FEM) is one of the popular techniques to evaluate the manufacturability of a given process design for a product [Wang and Tang, 1985; Lyu and Saitou, 2005; Johansson, 2008; Choi, et al. 2009]. In process capability analysis, Kazmer and Roser [1999] defined a capability index called “robustness index” for multiple simultaneous quality characteristics. Taguchi’s Signal-to-Noise S/N ratio [1986] is one of the commonly used methodologies. These indices depend on variation input and are computed directly from the output data of KPCs (Key Product Characteristics). On the other hand, design evaluation based on sensitivity analysis defines and develops input-independent ratios. One of the characteristics of sensitivity-based design evaluation is the characterization of product and process into Key Characteristics (KC). This line of research can be found in [Ceglarek, et al. 1994; Thornton, 1999] for single operation process and [Ding, 2002] for multi-station assembly process using state space approach.

Process evaluation using morphing for shape prediction can be found in recent research papers. Davis et al. [1996] predicted the wafer uniformity given discrete measurement points using thin-plate spline interpolation. Similar methodologies can also be found in Mahayotsanun et al. [2007] and Sah and Gao [2009] where TPS is

used to predict pressure distribution of the workpiece-tool interface in stamping sheet metal for process monitoring and control. Combining design and evaluation, Ryken and Vance [2000] developed a set of tools using virtual reality integrated with free form deformation and finite element analysis to facilitate the real-time design process of a tractor lift arm.

Process Monitoring and Control

The research on manufacturing process control focuses on the variation propagation analysis that investigates the variations accumulated through upstream stages and their impact on current and downstream stages. This line of research includes multistage variation propagation modeling [Mantripragada and Whitney, 1999; Jin and Shi, 1999; Djurdjanovic and Ni, 2001; Zhou, et al. 2003; Camelio, et al. 2003], model based process fault diagnosis [Ding, et al. 2002; Zhou, et al. 2004], as well as process adjustment with programmable toolings [Wang and Huang, 2007; Zhong, et al. 2009].

In these studies, surface shape are represented utilizing vectorial surface model [Huang, et al. 2003] or discrete nodes (obtained from CMM scanning) and corresponding processes are modeled using engineering knowledge such as kinematics for rigid bodies [Cai, et al. 1996] and finite element analysis for compliant parts [Camelio, et al. 2003], or by data driven approach [Apley and Shi, 2001; Liu, et al. 2008]. However, research on morphing methodologies in manufacturing process monitoring and control has not been attempted.

1.2.3. Summary of Literature Review

Shape changes are essential in most manufacturing processes. In manufacturing process design and evaluation, current research still focuses only on one product or product line. There is a lack of methodologies of using previously existed process information for process development of evolutionary products. For process control purpose, existing methodologies study discrete key product characteristics or surface vectors and have limitations in analyzing complex shape changes involving material properties and physical processes. Morphing is one promising method to facilitate process design for new product based on previous knowledge, as well as process monitoring and control by characterizing the interdependence of manufacturing stages. Although morphing algorithms have been widely used in computer graphics, filming, medical imaging, etc, it is rarely utilized in manufacturing process development. One concern is that the conventional morphing is data-driven and may not fully characterize a complex physical process that involves material, mechanics, process condition, etc. Therefore, there exists a need to extend from the geometry morphing to the aforementioned “functional morphing” and seek the opportunities in facilitating manufacturing process development and control.

1.3. RESEARCH OBJECTIVES

The objective of this research is to develop functional morphing methodologies and algorithms and explore the applications in manufacturing process development including process design, evaluation and control, specifically for the topics of stamping die development, formability evaluation and process control for multi-stage machining process. The research tasks include:

- 1) To develop methodologies for morphing based die face design of evolutionary product between its generations for sheet metal stamping process;
- 2) To develop a strain increment method for formability evaluation based on functional morphing;
- 3) To develop functional morphing based monitoring and control algorithms for multi-stage manufacturing process to improve process stability and reduce variation.

Fulfillment of the objectives will make it feasible to interpret shape changes based on physical attributes and process conditions, and further facilitate process development and improvement.

1.4. ORGANIZATION OF DISSERTATION

The organization of this dissertation is shown in Figure 1.4. Functional morphing algorithms are developed by integrating design data (geometric) and manufacturing information (physical) and then applied onto manufacturing process development including design evaluation, monitoring and control. This dissertation is presented in a multiple manuscript format. Chapter 2, 3 and 4 are written as individual research papers that are partially revised for this dissertation.

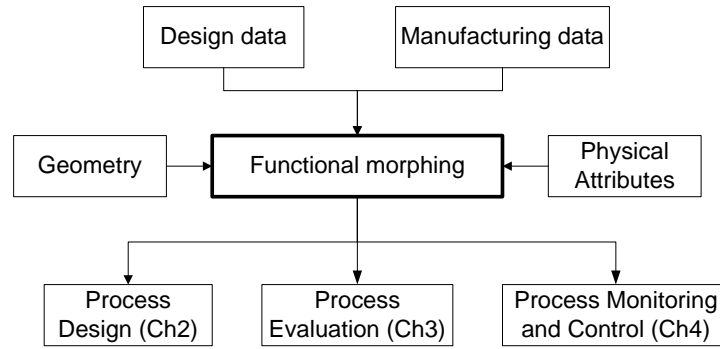


Figure 1.4 Research framework

Chapter 2 utilizes functional morphing for process design and proposes a new concept of evolutionary stamping die design based on functional morphing. The design method consists of a set of sequential steps of part-to-part mapping, die-to-die morphing and numerical verification. This concept integrates springback compensation by including a smoothness function during part-to-part mapping. Both 2D and 3D case studies are presented to illustrate the concept and procedure. The work was presented in a paper as [Zhou, et al. 2009].

Chapter 3 introduces a strain increment method based on functional morphing for early formability evaluation of a new product design by predicting strain distribution directly from the part-to-part mapping process. This method incorporates a bending energy constraint and a strain gradient penalty during morphing and thus makes the part-to-part mapping process equivalent to a boundary value problem and approximates the equilibrium state. It is shown, through a case study, that the strain field estimated by the proposed strain increment method compares well with that from the direct finite element analysis. Part of the work was presented in [Zhou, et al. 2009].

Chapter 4 develops a functional morphing model for manufacturing process control. This model characterizes the interdependence of downstream stages on the

surfaces that are generated during upstream stages and explores its applications in improving variation reduction strategy. It enables multi-scale variation propagation analysis and intermediate-stage process monitoring and further allows for accurate inter-stage adjustment that introduces shape deformation upstream to compensate for the errors downstream. A case study based on a two-stage machining process is demonstrated to illustrate the monitoring and compensation algorithms. This work will be published as [Zhou, et al. 2009].

Chapter 5 draws the conclusions and summarizes the original contributions of the dissertation. Several topics are also proposed for future research.

REFERENCES

- Anwarul, M. and Liu, M.C., (1995), "Optimal Manufacturing Tolerance: The Modified Taguchi Approach", *Proceedings of the Fourth Industrial Engineering Research Conference*, pp. 379-383.
- Apley, D. and Shi, J., (2001), "A Factor-Analysis Method for Diagnosing Variability in Multivariate Manufacturing Processes", *Technometrics*, Vol. 43, pp. 84-95.
- Bookstein, F.L., (1989), "Principal Warps: Thin-Plate Splines and the Decomposition of Deformations", *IEEE Transactions on Pattern Analysis and Machine Intelligence*, Vol. 11, pp. 567-585, 1989.
- Cai, W. and Hu, S.J., (1996), "Optimal Fixture Configuration Design for Sheet Metal Assembly With Spring Back", *Transactions of NAMRI/SME*, Vol. 23, pp. 229-234
- Cai, W., Hu, S.J. and Yuan, J.X., (1997), "A Variational Method of Robust Fixture Configuration Design for 3-D Workpieces", *ASME Transactions: Journal of Manufacturing Science and Engineering*, Vol. 119 (4), pp. 593-602.
- Camelio, J. and Hu, J., Ceglarek, D., (2003), "Modeling Variation Propagation of Multi-Station Assembly Systems with Compliant Parts", *ASME Transactions: Journal of Mechanical Design*, Vol. 125, pp. 673-681.
- Camelio, J., Hu, S.J. and Ceglarek, D., (2004), "Impact of Fixture Design on Sheet Metal Assembly Variation", *Journal of Manufacturing Systems*, Vol. 23 (3), pp. 182-193.

- Ceglarek, D., Shi, J. and Wu, S.M., (1994), "A Knowledge-Based Diagnostic Approach for the Launch of the Auto-Body Assembly Process", *ASME Transactions: Journal of Engineering for Industry*, Vol. 116, pp. 491-499.
- Choi, H.G.R., Park, M.H. and Salisbury, E., (2000), "Optimal Tolerance Allocation with Loss Function", *ASME Transactions: Journal of Manufacturing Science and Engineering*, Vol. 122 (3), pp. 529-535.
- Choi, K.S., Liu, W.N., Sun, X., Khaleel, M.A. and Fekete, J.R., (2009), "Influence of Manufacturing Processes and Microstructures on the Performance and Manufacturability of Advanced High Strength Steels", *Journal of Engineering Materials and Technology*, Vol.131.
- Coquillart, S., (1990), "Extended Free-form Deformation: A Sculpturing Tool for 3D Geometric Modeling," *ACM SIGGRAPH Computer Graphics*, Vol. 24, pp. 187-196.
- Davis, J.C., Gyurcsik, R.S., Lu, J.-C. and Hughes-Oliver, J.M., (1996), "A Robust Metric for Measuring Within-Wafer Uniformity", *IEEE Transactions on Components, Packaging, and Manufacturing Technology – Part C*, Vol. 19, pp. 283-289.
- Ding, Y., Ceglarek, D., and Shi, J., (2002), "Design Evaluation of Multi-station Assembly Processes by Using State Space Approach", *ASME Transactions: Journal of Mechanical Design*, Vol. 124, pp. 408-418.
- Ding, Y., Ceglarek, D., and Shi, J., (2002), "Fault Diagnosis of Multistage Manufacturing Processes by Using State Space Approach", *ASME Transactions: Journal of Manufacturing Science and Engineering*, Vol. 124 (2), pp. 313-322.
- Ding, Y., Jin, J., Ceglarek, D., and Shi, J., (2005), "Process-oriented Tolerancing for Multi-station Assembly Systems", *IIE Transactions*, Vol. 37, pp. 493-508.
- Djurdjanovic, D. and Ni, J., (2001), "Linear State Space Modeling of Dimensional Machining Errors", *Transactions of NAMRI/SME*, Vol. 29, pp. 541-548.
- Feng, C.X. and Kusiak, A., (1997), "Robust Tolerance Design with the Integer Programming Approach," *ASME Transactions: Journal of Manufacturing Science and Engineering*, Vol. 119 (44), pp. 603-610.
- Feng, C.X. and Kusiak, A., (2000), "Robust Tolerance Design with the Design of Experiments Approach", *ASME Transactions: Journal of Manufacturing Science and Engineering*, Vol. 122 (3), pp. 520-528.
- Galpin, F., Balter, R., Morin, L. and Deguchi, K., (2004), "3D Models Coding and Morphing for Efficient Video Compression", *Proceedings of the Conference on Computer Vision and Pattern Recognition*, Washington, DC.

- Hearn, D. and Baker, M.P., (1994), *Computer Graphics*. 2nd Edn., Prentice Hall.
- Hill, D.L.G., Batchelor, P.G., Holden, M. and Hawkes, D.J., (2001), "Medical Image Registration", *Physics in Medicine and Biology*, Vol. 46, pp. R1-R45.
- Hsiao, S.W. and Liu, M.C., (2002), "A Morphing Method for Shape Generation and Image Prediction in Product Design", *Design Studies*, Vol. 23 (6), pp. 533-556.
- Huang, Q. and Shi, J., (2003), "Simultaneous Tolerance Synthesis through Variation Propagation Modeling of Multistage Manufacturing Processes", *Transactions of NAMRI/SME*, Vol. 31, pp. 515-522.
- Huang, Q., Shi, J. and Yuan, J., (2003), "Part Dimensional Error and its Propagation Modeling in Multi-Stage Machining Processes," *ASME Transactions: Journal of Manufacturing Science and Engineering*, Vol. 125, pp. 255-262.
- Izquierdo, L.E., Hu, S.J., Du, H., Jin, R., Jee, H. and Shi, J., (2009), "Robust Fixture Layout Design for a Product Family Assembled in a Multistage Reconfigurable Line", *ASME Transactions: Journal of Manufacturing Science and Engineering*, Vol. 131.
- Jeang, A., (2002), "Optimal Parameter and Tolerance Design with a Complete Inspection Plan", *International Journal of Advanced Manufacturing Technology*, Vol. 20 (2), pp.121-127.
- Jeang, A. and Chang, C.L., (2002), "Concurrent Optimization of Parameter and Tolerance Design via Computer Simulation and Statistical Method", *International Journal of Advanced Manufacturing Technology*, Vol. 19 (6), pp. 432-441.
- Jin, J. and Shi, J., (1999), "State Space Modeling of Sheet Metal Assembly for Dimensional Control", *ASME Transactions: Journal of Manufacturing Science and Engineering*, Vol. 121, pp. 756-762.
- Johansson, J., (2008), "Manufacturability Analysis Using Integrated KBE, CAD and FEM", *Proceedings of the ASME International Design Engineering Technical Conferences and Computers and Information in Engineering Conference, DETC 2008*, Vol. 5, pp. 191-200.
- Kazmer, D. and Roser, C., (1999), "Evaluation of Product and Process Design Robustness", *Research in Engineering Design*, Vol. 11 (1), pp. 21-30.
- Kusiak, A. and Feng, C.X., (1996), "Robust Tolerance Design for Quality", *ASME Transactions: Journal of Engineering for Industry*, Vol. 118 (1), pp.166-169.
- Lee, J. and Haynes, L., (1987), "Finite Element Analysis of Flexible Fixturing System", *ASME Transactions: Journal of Engineering for Industry*, Vol. 109 (22), pp. 579-584.

- Lee, S., Wolberg, G., Chwa, K.Y. and Shin S.Y., (1996), "Image Metamorphosis with Scattered Feature Constraints", *IEEE Transaction on Visualization and Computer Graphics*, Vol. 2 (4), pp. 337-354.
- Li, M.H., (2000), "Quality Loss Function Based Manufacturing Process Setting Models for Unbalanced Tolerance Design", *International Journal of Advanced Manufacturing Technology*, Vol. 16 (1), pp. 39-45.
- Li, M.H., (2002), "Unbalanced Tolerance Design and Manufacturing Setting with Asymmetrical Linear Loss Function", *International Journal of Advanced Manufacturing Technology*, Vol. 20 (5), pp. 334-340.
- Li, Y. and Ni, J., (2009), "Constraints Based Nonrigid Registration for 2D Blade Profile Reconstruction in Reverse Engineering", *Journal of Computing and Information Science in Engineering*, Vol. 9.
- Liu, J., Shi, J. and Hu, S.J., (2008), "Engineering-Driven Factor Analysis for Variation Sources Identification in Multistage Manufacturing Processes", *ASME Transactions: Journal of Manufacturing Science and Engineering*, Vol. 130 (4), pp. 041009 1-10.
- Liu, W. and Yang, Y., (2007), "Multi-Objective Optimization of an Auto Panel Drawing Die Face Design by Mesh Morphing", *Computer-Aided Design*, Vol. 39, pp. 863-869.
- Lyu, N. and Saitou, K., (2005), "Topology Optimization of Multicomponent Beam Structure via Decomposition-Based Assembly Synthesis", *ASME Transactions: Journal of Mechanical Design*, Vol. 127, pp. 170-183.
- Mahayotsanun, N., Cao, J., Peshkin, M., Sah, S., Gao, R. and Wang, C.T., (2007), "Integrated Sensing System for Stamping Monitoring Control", *Proceedings of IEEE Sensors 2007 Conference*, San Diego, CA, pp. 1376-1379.
- Mantripragada, R. and Whitney, D.E., (1999), "Modeling and Controlling Variation Propagation in Mechanical Assemblies Using State Transition Models", *IEEE Transactions on Robotics and Automation*, Vol. 15, pp. 124-140.
- Menassa, R.J. and DeVries, W.R., (1991), "Optimization Methods Applied to Selecting Support Positions in Fixture Design", *ASME Transactions: Journal of Engineering for Industry*, Vol. 113 (4), pp. 412-418.
- Piegl, L.A. and Tiller, W., (2001), "Parameterization for Surface Fitting in Reverse Engineering", *Computer-Aided Design*, Vol. 33 (8), pp. 593-603.
- Ryken, M. and Vance, J. M., (2000), "Applying Virtual Reality Techniques to The Interactive Stress Analysis of a Tractor Lift Arm", *Finite Elements in Analysis and Design*, Vol. 35, pp. 141-155.

- Roth, B. and Crossley, W.A., (2003), "Application of Optimization Techniques in the Conceptual Design of Morphing Aircraft", *AIAA's 3rd Annual Aviation Technology: Integration, and Operations (ATIO)*, Denver, CO.
- Roth, B., Peters, C. and Crossley, W.A., (2002), "Aircraft Sizing with Morphing as an Independent Variable: Motivation, Strategies, and Investigations", *AIAA Paper* 2002-5840, Oct. 2002.
- Rueckert, D., Sonoda, L.I., Hayes, C., Hill, D.L.G., Leach, M.O. and Hawkes, D.J., (1999), "Nonrigid Registration Using Free-Form Deformations: Application to Breast MR Images", *IEEE Transactions on Medical Imaging*, Vol. 18 (8), pp.712- 721.
- Sah, S. and Gao, R.X., (2009), "Integrated Sensing of Pressure Distribution at The Workpiece-Tool Interface in Sheet Metal Stamping", *Proceedings of 2009 AMSE Manufacturing Science and Engineering Conference*, West Lafayette, IN, Paper No. MSEC2009-84342.
- Sarraga, R., (2004). "Modifying CAD/CAM Surfaces According to Displacements Prescribed at a Finite Set of Points", *Computer-Aided Design*, Vol. 36, pp. 343-349.
- Sederberg, T.W. and Parry, S.R., (1986), "Free-form Deformation of Polygonal Data", *Proceedings of International Electronic Image Week*, Nice, France, pp. 633-639.
- Shum, H.Y., Sing, B.K. and Chan, S.C., (2003), "Survey of Image-Based Representations and Compression Techniques", *IEEE Transactions on Circuits and Systems for Video Technology*, Vol. 13 (11), pp.1020-1037.
- Taguchi, G., (1986), *Introduction to Quality Engineering*, Asian Productivity Organization, Tokyo, Japan.
- Thornton, A.C., (1999), "A Mathematical Framework for the Key Characteristic Process", *Research in Engineering Design*, Vol. 11, pp. 145-157.
- Wang, H. and Huang, Q., (2007), "Using Error Equivalence Concept to Automatically Adjust Discrete Manufacturing Processes for Dimensional Variation Reduction", *ASME Transactions: Journal of Manufacturing Science and Engineering*, Vol. 129, pp. 644-652.
- Wang, M., Hu, H. and Qin, B., (2007), "Non-Rigid Medical Image Registration Using Optical Flow and Locally-Refined Multilevel Free Form Deformation", *Nuclear Science Symposium Conference Record*, Vol. 6, pp. 4552-4555.
- Wang, M.Y. and Pelinescu, D.M., (2001), "Optimizing Fixture Layout in a Point-Set Domain", *IEEE Transactions on Robotics and Automation*, Vol. 17 (3), pp. 312-323.

- Wang, N.M and Tang, S.C., (1985), *Computer Modeling of Sheet Metal Forming Processes: Theory, Verification and Application*, Metallurgical Society.
- Yin, Z., Song, J. and Jiang, S., (2004), “A New Strategy for Direct Generation of Tool Shape from a CAD Model Based on a Meshless Method”, *International Journal of Computer Integrated Manufacturing*, Vol. 17, pp. 327-338.
- Zhang, G., (1997), “Simultaneous Tolerancing for Design and Manufacturing”, *Advanced Tolerancing Techniques*, H. C. Zhang, ed., Wiley, New York, pp.207-231.
- Zhong, J., Liu, J. and Shi, J., (2009), “Predictive Control Considering Model Uncertainty for Variation Reduction in Multistage Assembly Processes”, *IEEE Transactions on Automation Science and Engineering*, Accepted as TASE-2009-091.
- Zhou, L., Hu, S.J. and Stoughton, T.B., (2009), “Formability Assessment in Stamping Die Face Morphing Using Strain Increment Method”, *Proceedings of the ASME International Manufacturing Science and Engineering Conference (MSEC 2009)*, West Lafayette, IN.
- Zhou, L., Hu, S.J., Stoughton, T.B. and Lin, G., (2009), “Evolutionary Stamping Die Development Using Morphing Technology”, *Transaction of NAMRI/SME*, Vol. 37.
- Zhou, L., Hu, S.J. and Stoughton, T.B., (2009), “Die Face Morphing with Formability Assessment”, submitted to *ASME Transactions: Journal of Manufacturing Science and Engineering*.
- Zhou, L., Wang, H. and Hu, S. J, (2009), “Functional Morphing in Complex Manufacturing Process and Its Applications in High-Definition Metrology Based Process Control”, to be submitted to *IEEE Transactions on Automation Science and Engineering*.
- Zhou, S., Chen, Y. and Shi, J., (2004), “Statistical Estimation and Testing for Variation Root-Cause Identification of Multistage Manufacturing Processes”, *IEEE Transactions on Robotics and Automation*, Vol. 1, pp. 73-83.
- Zhou, S., Huang, Q. and Shi, J., (2003) “State Space Modeling for Dimensional Monitoring of Multistage Machining Process Using Differential Motion Vector”, *IEEE Transactions on Robotics and Automation*, Vol. 19, pp.296-309.

CHAPTER 2

FUNCTIONAL MORPHING BASED EVOLUTIONARY STAMPING DIE DEVELOPMENT

ABSTRACT

Automotive die development is a lengthy process involving iterative steps of die-face engineering, virtual tryout through finite element analysis, and later, physical tryout. Such a process is also true for products that have been in the market for several generations. For these products, similarities are commonly identified among parts belonging to the same product family, or from one generation to the next. Such similarity allows the possibilities for the knowledge learned from the die design of one sheet metal product to be 'morphed' onto that of a new but similar product, and thus reducing those iterations and shortening product development time. In this chapter, a new concept for evolutionary die design is proposed using a functional morphing algorithm, in which the springback compensation information is considered through a smoothness function during the geometric morphing. This design method consists of a set of integrated steps of part-to-part mapping, die-to-die morphing and finite element verification. Both 2D and 3D case studies are presented to illustrate the concept and

Part of this chapter has been published as Zhou, L., Hu, S.J., Stoughton, T.B. and Lin, G., (2009), "Evolutionary Stamping Die Development Using Morphing Technology", *Transaction of NAMRI/SME*, Vol. 37.

procedure.

2.1. INTRODUCTION

In auto body development, forming is one of the most important manufacturing processes to achieve streamlined body and stylish appearance. In forming process development, Die Face Engineering (DFE) is the connection between design and manufacturing [Okamoto et al. 1988], which is the step for not only the parameterization from design concept to CAD models, but also the verification of feasibility that the designed part can be manufactured cost effectively. However, DFE is a very complicated and time-consuming procedure. Numerous iterations are usually needed because both the design specifications and the process feasibility (e.g., formability and springback) need to be balanced and satisfied. To facilitate and expedite the DFE process, systematic methodologies and tools need to be developed.

In vehicle families and product generations, similarities can be commonly identified among parts belonging to the same product family, or from one generation to the next (e.g. 1997-2003 vs. 2004-2007 or 2008 Chevy Malibu) (Figure 2.1). But, the current die design approach does not make full use of such similarity and still requires every step of DFE for each part in the new product generation. This process is not only expensive but also time consuming.



Figure 2.1 Product family of Chevy Malibu from 1997 to 2008

Morphing is a special effect in motion pictures and animations that changes one image into another through a seamless transition [Beier, et al. 1992]. Morphing has many applications in fields as diverse as computer animation, filming and medical imaging. Considering those similarities in product generations, morphing allows the possibility for the knowledge and experience learnt from the die-face design of one product (*Generation i*) to be ‘mapped/morphed’ onto that of a new but ‘similar’ product (*Generation i+1*), as shown in Figure 2.2. However, conventional morphing is data-driven and may not reflect the physical insights for process design. A *functional morphing* is therefore introduced to map the geometries. This functional morphing will pass the information including both geometric shape of die surface and the physical properties (feasibilities) such as springback compensation and formability.

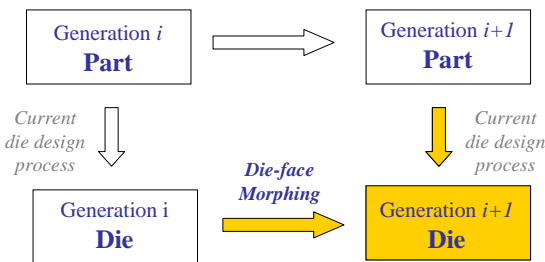


Figure 2.2 Mapping from old generation to new generation

In DFE, morphing has been utilized for springback compensation. Commercial software packages, such as *DynaForm* [ETA Inc. 2002], have included morphing algorithm to modify the mesh of a die based on the results of springback analysis. However, FE mesh is too rough to re-generate a smooth die surface for manufacturing. Therefore, direct modification of die surface was developed in recent studies. Sarraga [2004] developed a method for automatic CAD surface modification to fit point data obtained from the predicted springback. Application of morphing in autobody manufacturing has been demonstrated using the method. Different from Sarraga, a

meshless method was introduced for springback simulation by Yin [2004]. This method is more efficient since it generates the new die surface directly by avoiding the steps of meshing NURBS surface and separate finite element analysis.

However, very limited work exists in systematic evolutionary die design incorporating existing part/die information while integrating both geometry and physical constraints. Hence this chapter proposes a new concept of *evolutionary die design* using functional morphing. This design method consists of a set of integrated steps of part-to-part mapping, die-to-die morphing and finite element verification. Success of this method will facilitate faster design processes of new products by reducing iterations in the DFE process between design and manufacturing.

This chapter is organized as follows: Section 2.2 presents a method for die face morphing described by a sequence of part-to-part mapping, die-to-die morphing and numerical verification. Part geometry involving trimmed surfaces is also discussed. Section 2.3 presents a 2D case study of U-shaped channel stamping and a 3D case study of cup drawing using the proposed method. Section 2.4 summarizes the chapter with conclusions.

2.2. DIE FACE MORPHING ALGORITHM

Assume that the part geometries from generation i and new generation $i+1$ are known (Figure 2.2), denoted as the source and the target geometries. The existing part and new part are defined by Non-Uniform Rational B-Spline (NURBS) curves/surfaces, whose control points (CPs) and degrees of freedom (DOF) are both known. The following die morphing procedures are proposed, as shown in Figure 2.3:

- (1) A mapping function is obtained by functional morphing algorithm between the old part geometry and the new part geometry, represented by a set of NURBS control points. This registration is done by maximizing the correspondence between the two geometries where the mutual distance between the two surfaces is minimized.
- (2) Using the same mapping function obtained from part-to-part mapping, the old die geometry, which is also represented by a set of control points, is morphed onto the new die surface. In this die-to-die morphing, springback information from the previous generation die, which is reflected in the differences in shape between the previous part and previous dieface in the part area, is expected to be carried is expected to be carried into the next generation die.
- (3) For verification, forming analysis is conducted using finite element analysis (FEA) on the new morphed die. The part created by the morphed die is then compared with the desired part geometry. If the part generated by the morphed die is not within the design specification, then an iterative approach can be applied to find the optimal die face.

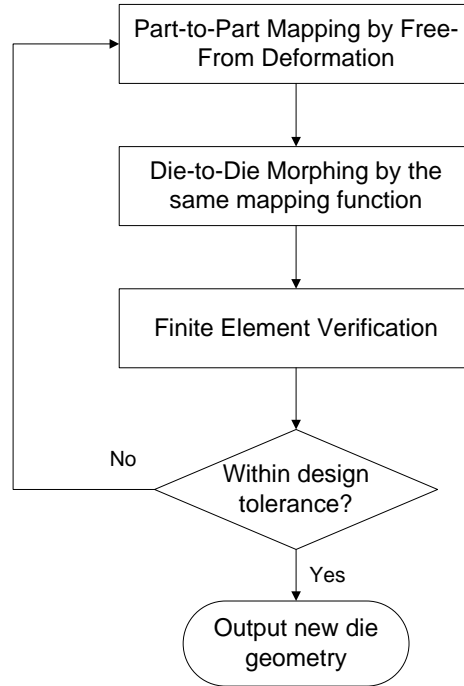


Figure 2.3 Die face morphing concept

2.2.1. Free-Form Representation for Part and Die

In stamping CAD design, the free-form geometries of the part and die are described by NURBS curves/surfaces [Mortenson 1985; Koivunen et al. 1995]. A NURBS curve has the mathematical form of,

$$S(\mathbf{P}) = \sum_{i=0}^n R_{i,p}(u) P_i, \quad R_{i,p} = \frac{N_{i,p} w_i}{\sum_{j=1}^k N_{j,p} w_j} \quad (2.1)$$

where $R_{i,p}(u)$ is the NURBS basis function of degrees of freedom p , w_i ($i = 1 \dots k$) are the corresponding weights, $N_{i,p}$ is the B-Spline basis function, $\mathbf{P} = [P_0 P_1 \dots P_n]$ are the n control points (CP), $\mathbf{U} = [u_0 u_1 \dots u_m]$ is the knot vector of m knots, and m, n, p satisfy $m = n + p + 1$.

A NURBS surface (Figure 2.4) is defined as,

$$S(\mathbf{P}) = \sum_{i=0}^{n_1} \sum_{j=0}^{n_2} R_{i,p}(u) R_{j,q}(v) P_{i,j} \quad (2.2)$$

where $R_{i,p}(u)$ and $R_{j,q}(v)$ are the NURBS basis functions of degrees of freedom p and q respectively, $P_{i,j}$ is the set of control points in a matrix form with dimensions $(n_1 + 1) \times (n_2 + 1)$, and $\mathbf{U} = [u_0 \ u_1 \ \dots \ u_{m_1}]$ and $\mathbf{V} = [v_0 \ v_1 \ \dots \ v_{m_2}]$ are the knot vectors in u and v directions. Here $m_1 = n_1 + p + 1$ and $m_2 = n_2 + p + 1$ also hold.

From Eqs. (2.1) and (2.2), it is seen that the shape of a curve/surface is fully determined by the locations of the set of CPs. By adjusting the locations of these CPs, the shape of the curve/surface can be changed, resulting in a new continuous curve/surface.

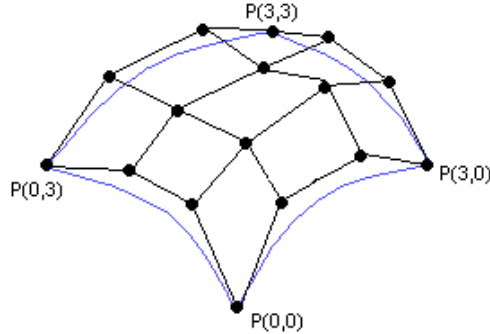


Figure 2.4 NURBS surface defined by 16 (4x4) control points

2.2.2. Part-to-Part Mapping by FFD Based Transformation

The part-to-part mapping is formulated by registering the source surface on an existing part to the target surface on a new part. The goal is to maximize the correspondence [Ko, et al. 2005] between these 2 surfaces. The surfaces are defined by two sets of CPs \mathbf{P}^S and \mathbf{P}^T correspondingly.

$$\mathbf{P}^S = \begin{bmatrix} \mathbf{P}_{11}^S & \cdots & \mathbf{P}_{1m_1}^S \\ \vdots & \ddots & \vdots \\ \mathbf{P}_{n_1}^S & \cdots & \mathbf{P}_{n_1m_1}^S \end{bmatrix} \mathbf{P}^T = \begin{bmatrix} \mathbf{P}_{11}^T & \cdots & \mathbf{P}_{1m_2}^T \\ \vdots & \ddots & \vdots \\ \mathbf{P}_{n_2}^T & \cdots & \mathbf{P}_{n_2m_2}^T \end{bmatrix} \quad (2.3)$$

This correspondence is usually measured using the general distance g_1 between the two surfaces, defined as,

$$g_1(\mathbf{P}^S, \mathbf{P}^T) = \left\| S \left[T \mathbf{P}^S \right] - S \mathbf{P}^T \right\|^2 \quad (2.4)$$

where $S \left[\mathbf{P}^T \right]$ is the target surface, $T(\cdot)$ is the transformation function on the CP set, and $S \left[T \mathbf{P}^S \right]$ is the surface defined by the transformed CP set \mathbf{P}^S . Maximizing the correspondence is equivalent to finding a transformation function $T(\cdot)$ to minimize the general distance $g_1(\mathbf{P}^S, \mathbf{P}^T)$. This transformation function is also referred as a part-to-part mapping function.

Cubic Free-Form Deformation (FFD) [Rueckert, et al. 1999] is selected as the transformation method since it is commonly used for localized geometry transformation in 3D space. The FFD is defined by a tensor-product of uniform cubic B-Spline blending functions in the form of

$$T(x, y, z) = \sum_{i=0}^3 \sum_{j=0}^3 \sum_{k=0}^3 B_i(u) B_j(v) B_k(w) \Phi_{i,j,k} \quad (2.5)$$

where, u, v, w are localized coordinates and B is the uniform cubic B-spline function.

$$\begin{aligned} u &= x - \lfloor x \rfloor \\ v &= y - \lfloor y \rfloor, \text{ and} \\ w &= z - \lfloor z \rfloor \end{aligned} \quad (2.6)$$

$$\begin{aligned}
B_0(t) &= (-t^3 + 3t^2 - 3t + 1) / 6 \\
B_1(t) &= (3t^3 - 6t^2 + 4) / 6 \\
B_2(t) &= (-t^3 + 3t^2 + 3t + 1) / 6 \\
B_3(t) &= t^3 / 6
\end{aligned}$$

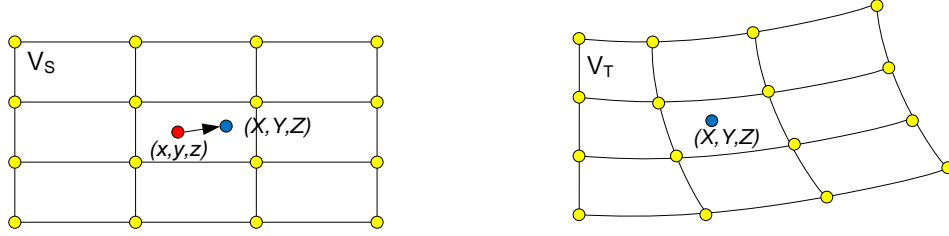


Figure 2.5 Free form deformation: (x,y,z) is the original point, (X,Y,Z) is the new point after FFD

The FFD transformation in Figure 2.5 defines a mapping $T: (x,y,z) \rightarrow (X,Y,Z)$ where (x,y,z) is from the source space V_S , and (X,Y,Z) is from the target space V_T . Φ is the set of lattice points (LP) in R^3 which define the space, i.e., the mesh grids.

Let $T^{(0)}$ denote an identity mapping from (x,y,z) to (x,y,z) , i.e.,

$$\begin{pmatrix} x \\ y \\ z \end{pmatrix} = T^{(0)}(x, y, z) = \sum_{i=0}^3 \sum_{j=0}^3 \sum_{k=0}^3 B_i(u) B_j(v) B_k(w) \Phi_{i,j,k}^{(0)} \quad (2.7)$$

where $\Phi_{i,j,k}^{(0)}$ can be regarded as the set of LPs which defines the original space and $T^{(0)}$ is the set of CPs defining the source surface. Let ΔT be the increment of the set of CP while $\Delta\Phi$ be the increment of set of LP during transformation which satisfies $\Delta\Phi = \Phi - \Phi^{(0)}$ and

$$T(x, y, z) = T^{(0)} + \Delta T$$

$$\sum_{i=0}^3 \sum_{j=0}^3 \sum_{k=0}^3 B_i(u) B_j(v) B_k(w) \Phi_{i,j,k} = \sum_{i=0}^3 \sum_{j=0}^3 \sum_{k=0}^3 B_i(u) B_j(v) B_k(w) \Phi_{i,j,k}^{(0)} + \Delta\Phi_{i,j,k} \quad (2.8)$$

Combining Eqs (2.7) and (2.8), it is seen that the difference between original CPs

and new CPs is fully determined by the movement of the corresponding lattice points $\Delta\Phi$.

$$\Delta T(x, y, z) = \sum_{i=0}^3 \sum_{j=0}^3 \sum_{k=0}^3 B_i(u)B_j(v)B_k(w)\Delta\Phi_{i,j,k} \quad (2.9)$$

In solving the part-to-part mapping, (x,y,z) is known as CP set \mathbf{P}^S and (X,Y,Z) is known as CP set $\tilde{\mathbf{P}}^S$, which contains the optimal locations of the CPs of the source object after achieving the maximum correspondence to the target object. Therefore,

$$\mathbf{P}^S = T^{(0)}(x, y, z) \text{ and } \tilde{\mathbf{P}}^S - \mathbf{P}^S = \Delta T(x, y, z) \quad (2.10)$$

From Eqs (2.4), (2.9) and (2.10), the objective g_1 is a function of $\Delta\Phi_{i,j,k}$, the movement of the LP set. Therefore, $\Delta\Phi_{i,j,k}$ defines the mapping between the existing part surface and the new part surface.

FFD based functional morphing for registration

The mathematical goal of the registration is to find a mapping function by moving the lattice points $\Delta\Phi_{i,j,k}$ to warp the space V_S to the space V_T , so that the general distance between the transformed source object and the target object is minimized. The optimization problem can be formulated as,

$$\begin{aligned} \mathbf{Min}_{\Delta\Phi} g_1(\mathbf{P}^S, \mathbf{P}^T) &= \left\| S \begin{bmatrix} T & \mathbf{P}^S \end{bmatrix} - S \mathbf{P}^T \right\|^2 \\ \mathbf{s.t.} & \\ g_1(\mathbf{P}^S, \mathbf{P}^T) &\leq \varepsilon \end{aligned} \quad (2.11)$$

where $\Delta\Phi$ is the optimization variable and ε is the maximum registration error. The optimal locations of CPs $\tilde{\mathbf{P}}^S$ are obtained by minimizing the general distance g_1 between the transformed source object and the target object.

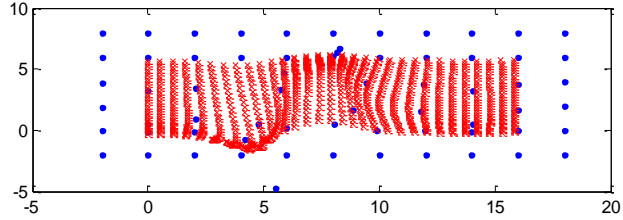
Optimization (2.11) only considers the mapping of a pure geometric relationship. It is also noticed that the solution to the optimization is not unique because there are usually more variables than the number of equations. The non-uniqueness of the solution provides a means to overcome the problem that some of the solutions are not physically feasible. One example is shown in Figure 2.6(A), where the red points inside the FFD volume indicate the movement after morphing. It is seen that without a smoothing function, some points are overlapped with others. This solution is feasible under pure geometric mapping; however, such overlapping of material is infeasible for a physical process. Therefore, a smoothing function J is introduced to the previous objective function (2.11), which has the form of [Sarraga 2004],

$$J = \int L(f) du dv dw \quad (2.12)$$

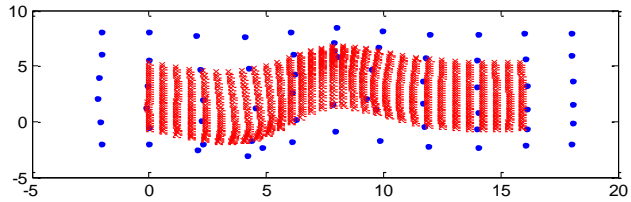
where,

$$L(f) = \left(\frac{\partial^2 \Delta T}{\partial u^2} \right)^2 + \left(\frac{\partial^2 \Delta T}{\partial v^2} \right)^2 + \left(\frac{\partial^2 \Delta T}{\partial w^2} \right)^2 + \left[\left(\frac{\partial^2 \Delta T}{\partial u \partial v} \right)^2 + \left(\frac{\partial^2 \Delta T}{\partial v \partial w} \right)^2 + \left(\frac{\partial^2 \Delta T}{\partial w \partial u} \right)^2 \right]$$

$$\Delta T(x, y, z) = \sum_{i=0}^3 \sum_{j=0}^3 \sum_{k=0}^3 B_i(u) B_j(v) B_k(w) \Delta \Phi_{i,j,k}$$



(A) Without including smoothing function



(B) With including smoothing function

Figure 2.6 Comparison with and without including smoothing function

Figure 2.6(B) shows the deformation with the smoothing function from the same objective function. A smoother morphing result is given by including such a function. Figure 2.6(B) indicates that inside the FFD volume, the material near the object to be registered will move in the similar direction, resulting in a smooth deformation. In the stamping die development, the die surface deviates from part surface for springback compensation. If the parts from 2 generations are similar in terms of strain path during stamping, by applying the functional morphing of combined geometric mapping and smoothness, this springback information will be carried from the prior generation die into the new generation.

Combining Eqs. (2.11) and (2.12), a final optimization problem (2.13) is defined,

$$\mathbf{Min}_{\Delta\Phi} (1-\alpha)g_1(\mathbf{P}^S, \mathbf{P}^T) + \alpha \cdot J \quad (2.13)$$

$$= (1-\alpha) \cdot \left\| S \begin{bmatrix} T & \mathbf{P}^S \end{bmatrix} - S \mathbf{P}^T \right\|^2 + \alpha \cdot \int L(f) dudvdw$$

s.t.

$$g_1(\mathbf{P}^S, \mathbf{P}^T) \leq \varepsilon$$

where,

$$S(\mathbf{P}) = \sum_{i=0}^{n_1} \sum_{j=0}^{n_2} N_{i,p}(u) N_{j,q}(v) P_{i,j}$$

$$T(x, y, z) = \sum_{i=0}^3 \sum_{j=0}^3 \sum_{k=0}^3 B_i(u) B_j(v) B_k(w) \Phi_{i,j,k}^{(0)} + \Delta\Phi_{i,j,k}$$

$$\mathbf{P}^S = T^{(0)}(x, y, z) = \sum_{i=0}^3 \sum_{j=0}^3 \sum_{k=0}^3 B_i(u) B_j(v) B_k(w) \Phi_{i,j,k}^{(0)}$$

$$L(f) = \left(\frac{\partial^2 \Delta T}{\partial u^2} \right)^2 + \left(\frac{\partial^2 \Delta T}{\partial v^2} \right)^2 + \left(\frac{\partial^2 \Delta T}{\partial w^2} \right)^2 + \left[\left(\frac{\partial^2 \Delta T}{\partial u \partial v} \right)^2 + \left(\frac{\partial^2 \Delta T}{\partial v \partial w} \right)^2 + \left(\frac{\partial^2 \Delta T}{\partial w \partial u} \right)^2 \right]$$

In this optimization problem, α is a weight valued between 0 and 1, representing a

trade-off between the correspondence and the morphing smoothness. Since Eq. (2.13) is a non-linear optimization problem, an iterative numerical method is applied to solving the problem.

2.2.3. Die-to-Die Morphing

The mapping function between the part surfaces is then used to generate the new die surface given an existing, *generation i*, die. Such a function, obtained by solving $\Delta\Phi$ in the optimization problem (2.13), is then applied on the geometry of the existing die surface, which is also defined by a set of CPs, to generate the new die surface.

Morphing of the die surface is done through free form deformation,

$$\Delta T(x_d, y_d, z_d) = \sum_{i=0}^3 \sum_{j=0}^3 \sum_{k=0}^3 B_i(u_d) B_j(v_d) B_k(w_d) \Phi^{(0)}_{i,j,k} + \Delta\Phi_{i,j,k} \quad (2.14)$$

where (u_d, v_d, w_d) are local coordinates corresponding to the global coordinates (x_d, y_d, z_d) of the control points from the existing die face, $\Phi^{(0)}_{i,j,k}$ are the LPs to define the original FFD volume space while $\Delta\Phi_{i,j,k}$ is the increment of LPs to define the part-to-part mapping. Finally, the new die surface generated by Eq. (2.14) is verified using finite element method and the result is compared with the desired part shape.

2.2.4. Consideration on Trimmed Surfaces

More complex product shape (surfaces) cannot be represented by NURBS surfaces with their control points defined in a matrix form (Eq. (2.3)). In such a case, trimmed surface is used which consists of both a NURBS surface and closed loop boundaries. Trimmed surface is commonly used for the representations of feature edges and the connection between multiple surface patches. For example, the green

surface shown in Figure 2.7 has a feature edge on the top right corner. It is trimmed from the original NURBS surface (blue surface) by a close-loop boundary (red lines).

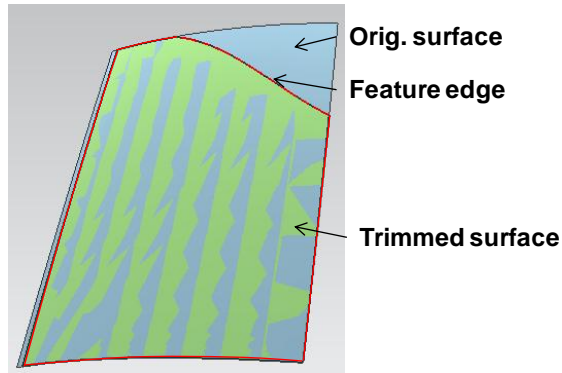


Figure 2.7 Sample of trimmed surface

In the Initial Graphics Exchange Specification (IGES) [IGES/PDES Organization, 1997], boundaries lines/curves are defined by a set of 2D B-spline curves in local coordinate system between 0 and 1. For example, a regular B-spline surface consists of 4 straight lines with coordinates (0,0)-(1,0), (1,0)-(1,1), (1,1)-(0,1) and (0,1)-(0,0). The sample surface shown above has the boundary lines plotted in Figure 2.8. It is seen that there are 5 boundary lines connected together to trim the original NURBS surface.

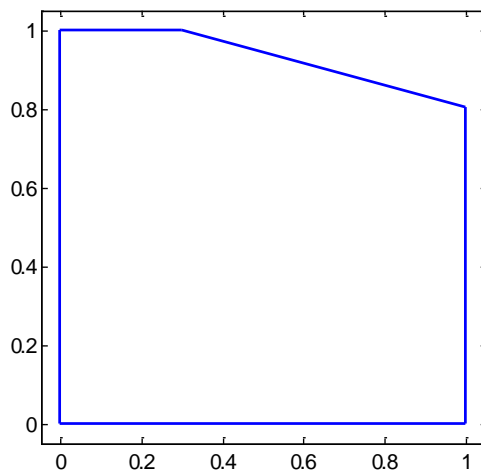


Figure 2.8 Boundary lines of sample trimmed surface

In die face morphing for trimmed surfaces, the mapping function needs to include

the boundaries, so that in the die-to-die morphing step, the morphed new die surface can also be trimmed to produce the desired part. Therefore, the following part-to-part mapping including boundary mapping is proposed:

- 1) Solve part-to-part mapping from Eq.(2.13) using the untrimmed source surface to register with target surface. This step is the same as the mapping of untrimmed surfaces.
- 2) Project the boundary points of target (points cloud) onto the transformed source surface and cluster them into groups. The number of groups equals to the number of boundary lines/curves. In this step, statistical clustering techniques can be used to group these boundary points on the transformed source surface, e.g., K-Means [Johnson and Wichern, 2001] is one of the efficient methods to cluster the spatial distributed points.
- 3) Fit each group of boundary points to a spline in the local coordinate to obtain the boundary curves. These boundary curves can be further used to trim the morphed dies accordingly and generate new die surface.

A case study utilizing the proposed method will be demonstrated in Section 2.3.3.

2.3. CASE STUDY

2.3.1. 2D Study on Stamping U-shaped Channel

A stamping process for a U-shaped channel is shown in Figure 2.9 (A, B) with the original part and die geometries both known. A concave feature is added onto the part shape (Figure 2.9 (C)). The proposed morphing method is applied to generate a new die shape for the new part.

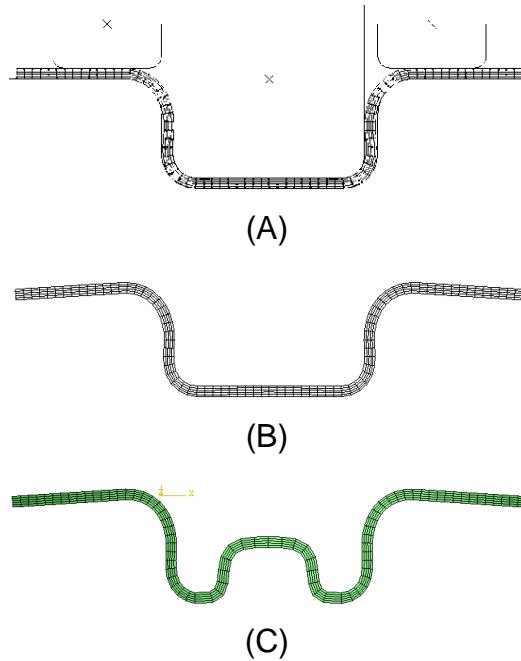
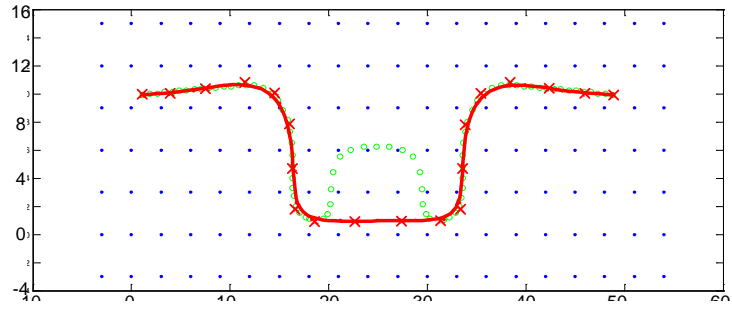


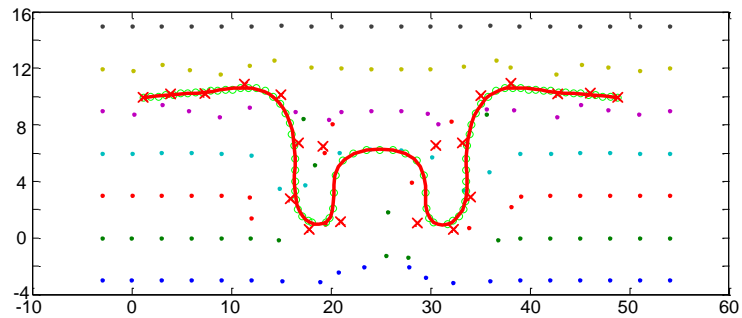
Figure 2.9 (A) original die; (B) original part after springback; (C) desired new part with a concave feature at bottom (after springback)

A 3rd order NURBS curve with 20 CPs is adopted to represent the original part shape. The first step is to set up the mapping between the old part geometry to the new part geometry by optimization of the objective function defined in Eq. (2.13). The optimization parameter α is chosen to be 0.05.

The mapping result is shown in Figure 2.10. $\Delta\Phi$ is solved by iterative searching for the optimal solution of the objective equation. Then, the old die geometry is morphed using the same mapping function shown in Figure 2.11 to obtain the new die.



(A) Initial state



(B) After Mapping

Figure 2.10 Part-to-part mapping (dots: lattice points, cross: control points of morphed original part, circle: desired new part, line: NURBS curve generated from the control points)

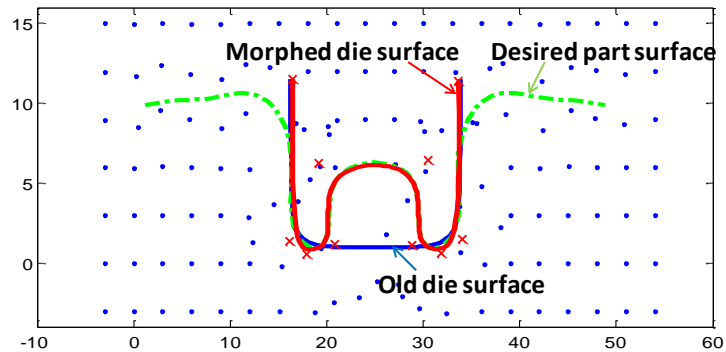


Figure 2.11 Die-to-die morphing (dots: lattice points, Cross: control points of the morphed die, solid line: Die surface, dashed line: desired part surface)

For the verification of the new die surface generated by the procedure, an FE analysis is performed by extracting and meshing the die geometry. The simulation environment is *ABAQUS 6.8* with Explicit and Standard solver [ABAQUS Inc. 2008]. The material model is elastic/plastic using aluminum alloy AA6111-T4. The material

properties are listed in Table 1. The forming analysis is conducted explicitly, in which the aluminum blank is free to be drawn with friction condition specified between blank and blank holder and between blank and die. A static analysis is used for springback estimation by releasing the constraints from the die.

Table 2.1 Material properties of AA6111-T4

Young's Modulus (GPa)	70
Poisson's Ratio	0.33
Yield Stress (MPa)	140
Plasticity	Flow rule

For comparison, the part generated from the morphed new die surface and the desired part are plotted in Figure 2.12 (after springback). It is observed that the new die surface can capture the concave feature added to the original geometry by the proposed morphing method. Moreover, springback analysis shows that the springback of the new part generated by morphing old die is similar to that from the desired part.

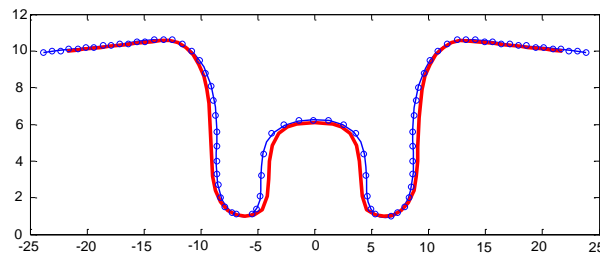


Figure 2.12 Comparison of the part generated from the morphed die (solid line) to the desired part (circled line)

2.3.2. 3D Case Study on Cup Drawing

A cup drawing case study is conducted to demonstrate the die face morphing method in 3D. The new part shape is modified from the original part shape (Figure 2.13

(A)) by adding an increased stamping depth and a concave bottom (Figure 2.13 (B)). Since it is a symmetric structure, only 1/8 of the model is model shown in Figure 2.13 (C). It should be noticed that the existing part is after springback from a flat flange die, therefore, the flange of the existing part is not flat. In the new part design, it is required the flange after springback is flat, as shown in Figure 2.13 (C). A matrix of (25×7) CPs NURBS surface is used to represent the surface of the part.

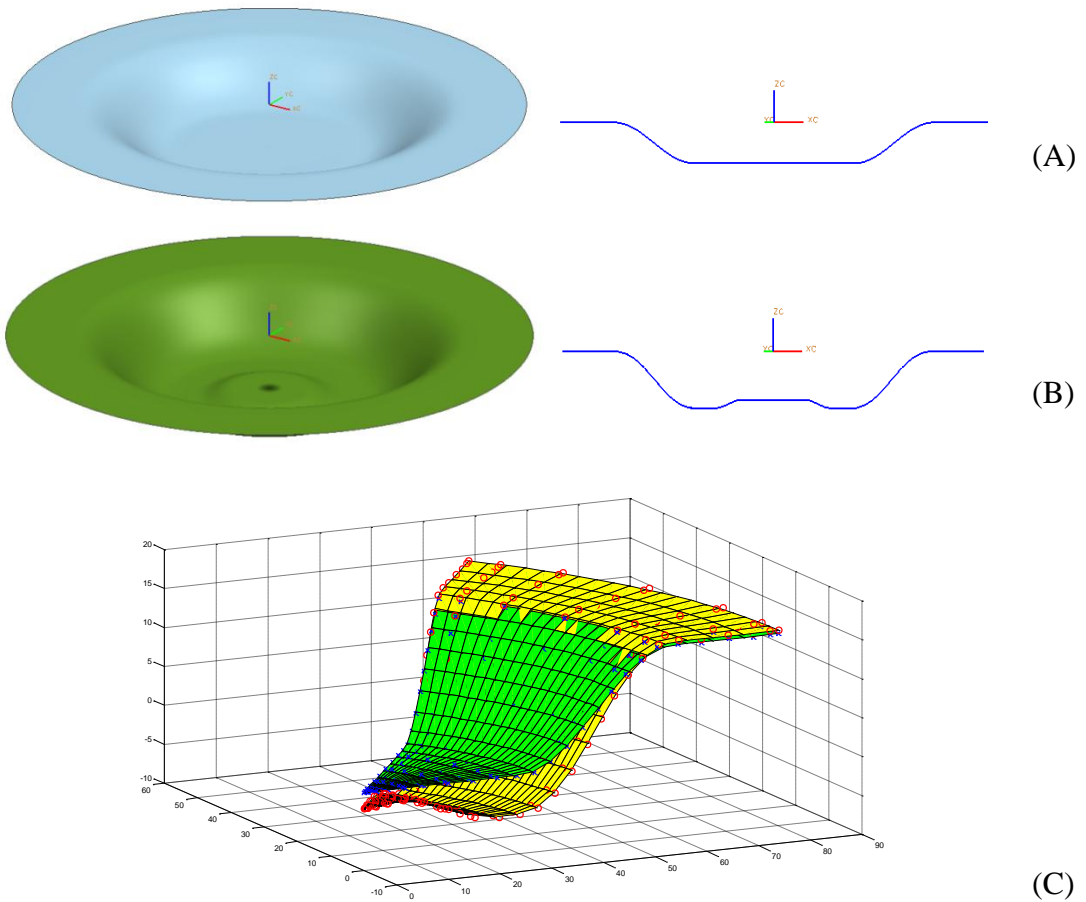


Figure 2.13 3D cup drawing case study: (A) shape of the existing part; (B) shape of the new part; (C) 1/8 modeling. (x: NURBS control points of the existing part, o: NURBS control points of the new part)

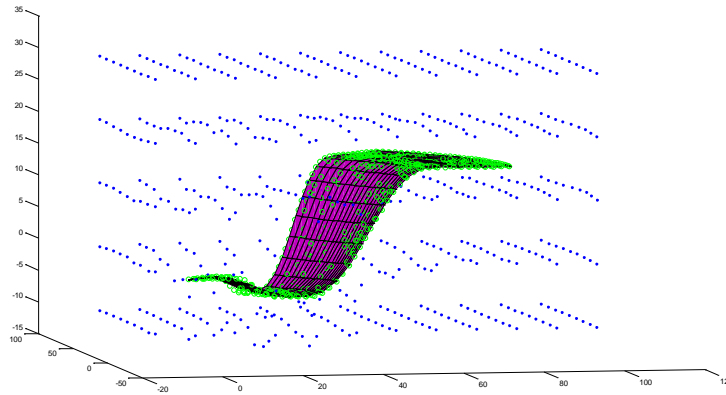


Figure 2.14 Part-to-part mapping of 3D cup drawing

The part-to-part mapping function is obtained by solving the optimization problem defined in Eq.(2.13). Figure 2.14 shows the mapping between the existing part and the new part. By close inspection on the movements of all LPs, the volume space is moved downward to match the existing part to the new part.

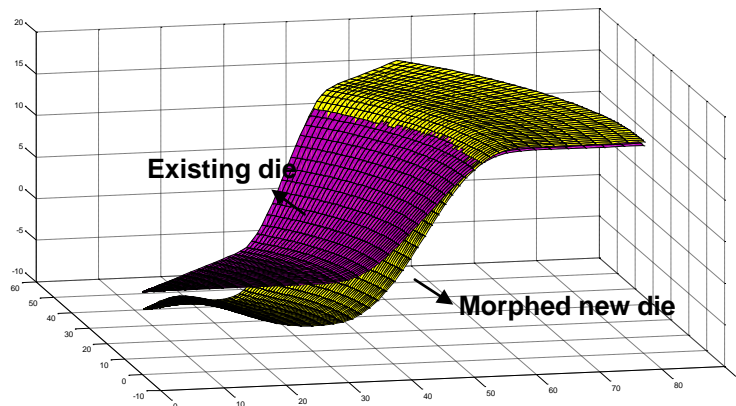


Figure 2.15 The new die face generated from the evolutionary die morphing method

The new die face is generated by using the same mapping function, as shown in Figure 2.15. A finite element modeling is then conducted using the morphed die geometry to further compare the part generated by the morphed die face and the desired part. Both explicit stamping process and implicit springback analysis have been

performed. Figure 2.16 shows the comparison of the nodes from FEA results and the surface of the desired part. It is seen that the part generated by the morphed die captures both features (increased draw depth and concave bottom) added to the original part and the springback in terms of the flange shape, where the new part has a flat flange as desired.

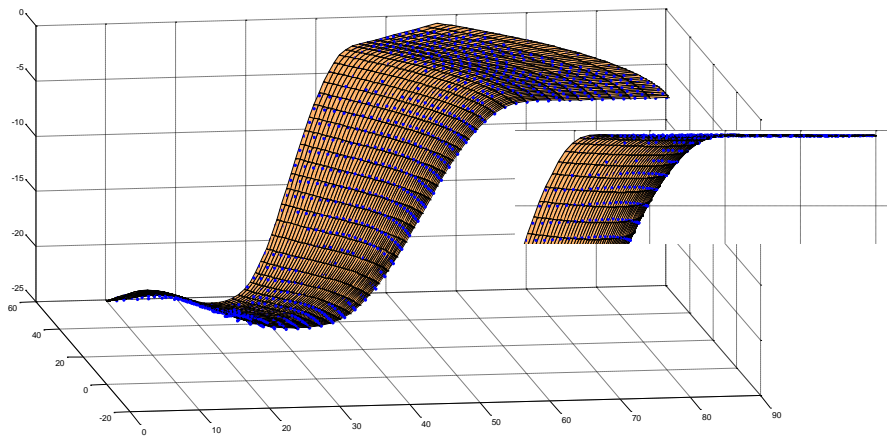
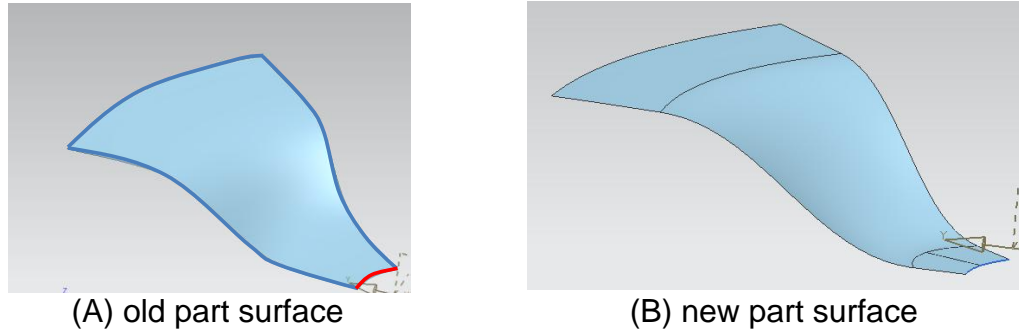


Figure 2.16 Comparison of the part generated by the morphed die (point cloud) and the desired part (surface)

2.3.3. Mapping of Trimmed Surface

One challenge proposed in Section 2.2.4 is to deal with trimmed surfaces, in which part-to-part mapping function will consist of 2 parts: NURBS surface mapping and boundary mapping. A similar cup drawing case study is shown in Figure 2.17 with a hole in the middle, in which the hole is trimmed from the original NURBS surface (only a 1/8 of the surface is shown). The new surface has both increased draw depth and hole diameter as shown in Figure 2.17(B).

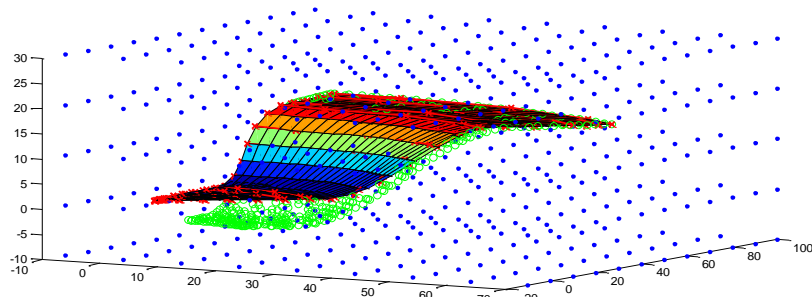


(A) old part surface

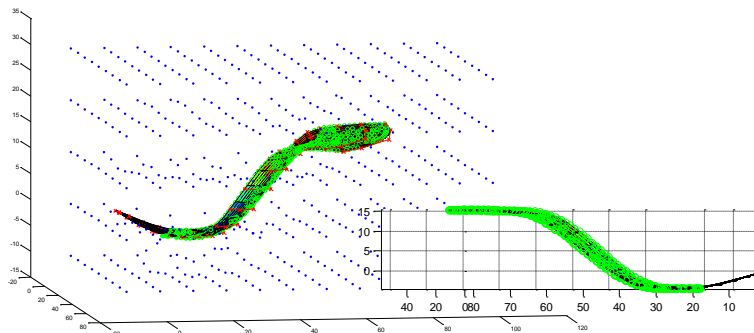
(B) new part surface

Figure 2.17 Case study of trimmed surfaces mapping

Part-to-part mapping function starts from registering the original NURBS surface of the old part to the new part. The original surface of the existing part is a full cup without the hole in the middle (Figure 2.18(A)). After registration, only the trimmed part areas are matched between old and new parts, while the tip area which is trimmed from the old part surface deforms in the way to improve the smoothness (Figure 2.18(B)).



(A) before part-to-part mapping (surface: untrimmed existing part; circle: new part surface; cross: control points to be mapped)



(B) after part-to-part mapping (surface: untrimmed existing part; circle: new part surface; cross: control points to be mapped)

Figure 2.18 Part-to-part mapping for trimmed surfaces

Clustering method, e.g., K-Means, is utilized to group the boundary nodes. The number of groups is determined by maximum Silhouette value. Result from K-Means analysis shown in Figure 2.19 indicates that there are 5 groups, although 2 groups are suggested on the left border. The boundary points in each group are then fitted into a B-spline curve.

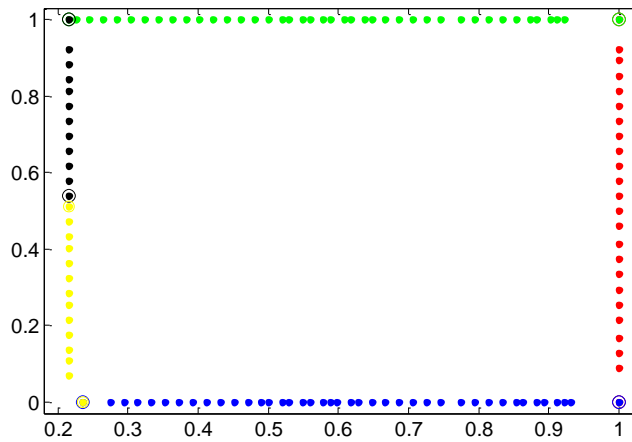


Figure 2.19 Boundary groups by K-Means

Finally, the new die surface is morphed using the same mapping function from the old die surface and then trimmed by the fitted boundaries, as shown in Figure 2.20.

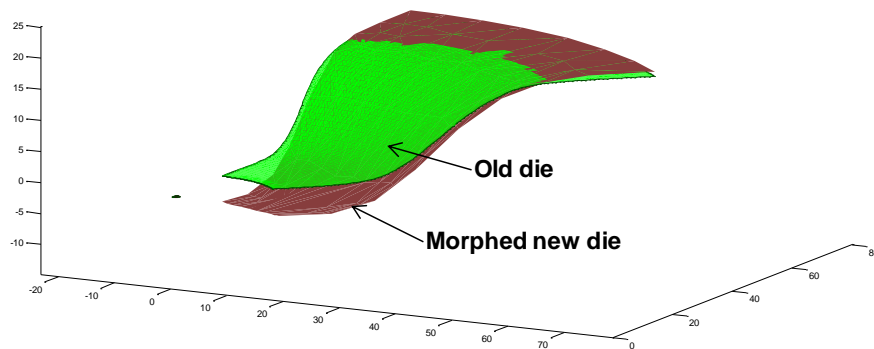


Figure 2.20 Die face morphing for trimmed surface

2.4. CONCLUSION

A new concept using functional morphing for evolutionary die development has been proposed using three sequential steps: part-to-part mapping between the existing part and the new part, die-to-die morphing using the same parts mapping function, and finite element verification. The following conclusions are drawn:

- 1) A part-to-part mapping function is established between the part surfaces from two generations by solving the optimization problem (2.13) based on functional morphing. This functional morphing allows geometric mapping with physical feasibility, in which the smoothness function helps inherit the springback compensation from previous generation die to the new generation.
- 2) Methodology for trimmed surfaces morphing is proposed by including a mapping function of original NURBS surfaces and a boundary mapping. Statistical clustering method, e.g. K-Means, can be used to group boundary points to fit B-spline boundary curves.
- 3) Both 2D and 3D case studies show that, the feature change in the new part can be captured by the part generated by the morphed die using the same part-to-part mapping function. Springback is also found similar to the desired part.

REFERENCES

- ABAQUS Inc. (2008). ABAQUS User's Manual.
- Beier, T. and Shawn, N., (1992), "Feature-Based Image Metamorphosis", *Computer Graphics*, Vol. 26 (2), pp. 36-42.

- ETA Inc., (2002), *Dynaform-PC User's Manual*, Engineering Technology Associates, Inc.
- IGES/PDES Organization, (1997), "Initial Graphics Exchange Specification IGES 5.3", U.S. Product Data Association.
- Johnson, R. A. and Wichern, D.W., (2001), "Applied Multivariate Statistical Analysis", 5th Edn., Prentice Hall, New York.
- Ko, K., Maekawa and T., Patrikalakis, N., (2005), "Algorithms for Optimal Partial Matching of Free-Form Objects with Scaling Effects", *Graphical Models*, Vol. 67, pp. 120-148.
- Koivunen, V. and Bajcsy, R., (1995). "Spline Representations in 3-D Vision", *Proceedings of International NSF-ARPA Workshop on Object Representation in Computer Vision*, pp. 177-190.
- Mortenson, M., (1985), *Geometric modeling*. John Wiley & Sons, Inc., New York.
- Okamoto, I., Takahashi, A., Sugiura, H., Yamada, N. and Mori, T., (1988). "Computer Aided Design and Evaluation System for Stamping Dies at Toyota", *SAE Publication: Advances and Trends in Automotive Sheet Steel Stamping*, Vol. 206, pp. 79-89.
- Rueckert, D., Sonoda, L., Hayes, C., Hill, D., Leach, M. and Hawkes, D., (1999), "Nonrigid Registration Using Free-Form Deformations: Application to Breast MR Images", *IEEE Transactions on Medical Imaging*, Vol. 18, pp. 712-721.
- Sarraga, R., (2004). "Modifying CAD/CAM Surfaces According to Displacements Prescribed at a Finite Set of Points", *Computer Aided Design* , Vol. 36, pp. 343-349.
- Yin, Z., Song, J. and Jiang, S., (2004), "A New Strategy for Direct Generation of Tool Shape from a CAD Model Based on a Meshless Method", *International Journal of Computer Integrated Manufacturing* , Vol. 17, pp. 327-338.

CHAPTER 3

FUNCTIONAL MORPHING BASED FORMABILITY ASSESSMENT IN STAMPING DIE FACE MORPHING USING STRAIN INCREMENT METHOD

ABSTRACT

A strain increment method is proposed for early formability assessment in die face engineering by predicting the strain distribution directly from the part-to-part mapping process based on functional morphing. This method consists of mapping the finite element mesh to the geometry of an existing part, solving the part-to-part mapping relation by functional morphing integrating a bending energy and strain gradient penalty functions, and extracting strain increment from the part-to-part mapping related displacement field. Case studies show that the strain field obtained using the proposed strain increment method compares well with that from the finite element analysis. Since this method does not require knowledge of the new die surface, such formability assessment can serve as an early manufacturing feasibility analysis on the new part design.

Contents of this chapter have been published as Zhou, L., Hu, S.J. and Stoughton, T.B., (2009), "Formability Assessment in Stamping Die Face Morphing Using Strain Increment Method", *Proceedings of the ASME International Manufacturing Science and Engineering Conference (MSEC 2009)*, West Lafayette, IN. and submitted to ASME Transactions: *Journal of Manufacturing Science and Engineering* under Zhou, L., Hu, S.J. and Stoughton, T.B., (2009), "Die Face Morphing with Formability Assessment".

3.1. INTRODUCTION

In vehicle families and product generations, similarities can be commonly identified among parts belonging to the same product family, or from one generation to the next. Such similarities can be utilized to facilitate and expedite the DFE process using evolutionary stamping die face morphing [Zhou, et al. 2009]. Die face morphing allows the knowledge learned from the die design of one sheet metal product to be functionally morphed onto that of a new but similar product inheriting the springback information from the existing die. The die morphing approach includes three sequential steps: 1) part-to-part mapping based on the geometric relationship between an existing part and a new part, 2) die-to-die morphing using the part mapping function obtained in Step 1, and 3) finite element verification of the morphed die.

The computational steps from evolutionary stamping die morphing can also be applied to predicting the formability of sheet metals products. The displacement field solved from the part-to-part mapping step in the evolutionary stamping die morphing algorithm satisfying physical feasibility can be utilized to extract the strain increment from one generation of product to the next. Then the strain distribution of the new product can be estimated based on the strain of the old product and the strain increment. In this chapter, the geometry and formability information (i.e., strain distribution) from an existing design are integrated into the morphing process to estimate the formability (i.e., strain distribution) for the new part. A strain increment method is then proposed to predict the strain distribution without the new die geometry being available. This method is based on the functional morphing concept in that bending energy of the FFD volume and a strain gradient regularization term are introduced into geometric

mapping. The formability can be further assessed through strain or stress based approaches using the estimated strain distribution for the new part. Such an early assessment is beneficial to both design and DFE engineers in reducing the design/manufacturing iterations.

This chapter is organized as follows: Section 3.2 reviews current direct methods for strain estimation in sheet metal forming. In Section 3.3, a strain increment method is proposed to predict the strain distribution of the new part by integrating a bending energy function and a strain gradient penalty. This method is then demonstrated in Section 3.4 by two case studies of a 2D U-shaped channel stamping and a 3D cup drawing.

3.2. STATE-OF-THE-ART

Strain distribution is critical in determining the formability of the sheet metal product in the stamping process. Traditional methods of stamping die development include trial-and-error which is time consuming and expensive. With the advancement in computer technology, numerical methods can provide faster and cost effective estimation of forming process and are now widely adopted in forming design and manufacturing [Kobayash, et al. 1989; Saran, et al. 1990; Chen and Chiang, 1998; Lin, et al. 2007]. However, most of the current analysis methods require interaction between design and DFE stages: trial dies have to be developed in order to simulate the forming process and then verify the manufacturability of the designed part. If the manufacturing specification is not met, engineering changes have to be made on the part design.

In order to reduce the iteration between design and DFE, some direct prediction methods have been developed to predict the strain distribution directly from part design. Such methods include ideal forming theory and inverse approach (one-step solution). The ideal forming theory [Chung and Richmond, 1992, 1994; Chung, et al. 1997] is developed based on the principle of extremum work. In this approach, each individual material element is locally prescribed to deform in a minimum work path and the ideal global process is then defined as the one having optimal global plastic work in a final shape. The inverse approach [Guo, et al. 1990, 2000; Naceur, et al. 2004] is based on the principle of virtual work. It discretizes the part surface by triangular facet shell elements and computes the inverse deformation tensor to estimate the large logarithmic strain and predict the initial blank shape. Applications using both methods have been successfully demonstrated [Sabourin, et al. 2004; Lan, et al. 2005; Ryou, et al. 2005].

For the design of evolutionary products, both direct methods are capable of estimating the strain or formability at the design stage without DFE. However, both methods require generating new finite element mesh once the part design is changed. Considering the geometric similarity of sheet metal products within the same product family or in multiple generations, more efficient algorithm can be developed if such similarity information is utilized. With the implementation of geometric modeling such as morphing on product design [Hong, et al. 2006; Chen, et al. 2003], morphing methodology has shown great potential in evolutionary stamping die development. An evolutionary die face morphing concept was recently developed using functional morphing [Zhou, et al. 2009] for the stamping process development of metal products

from the same product family or different product generations. This functional morphing algorithm maps geometries between part geometries considering springback compensation. Based on this morphing algorithm, methodologies for strain estimation of the similar parts from the same product families is to be developed in this chapter.

3.3. THE STRAIN INCREMENT METHOD

3.3.1. Geometric Mapping by Free-Form Deformation

The part-to-part mapping procedure as proposed by Zhou, et al. [2009] is briefly reviewed here. Assume that the part geometries from an existing generation, i , and a new generation, $i+1$, are known. The existing part and new part are defined by Non-Uniform Rational B-Spline (NURBS) curves/surfaces whose control points (CPs) and degrees of freedom (DOF) are both known. A mapping function, denoted as part-to-part mapping, is obtained by registration between the existing part geometry and the new part geometry. This mapping function, defined by the movement ($\Delta\Phi$) of Free-form deformation (FFD) [Sederberg and Parry, 1986] lattice points, is solved by introducing an optimization problem as below:

$$\mathbf{Min}_{\Delta\Phi} g_1(\mathbf{P}^S, \mathbf{P}^T) = \left\| S \begin{bmatrix} T & \mathbf{P}^S \end{bmatrix} - S \mathbf{P}^T \right\|^2 \quad (3.1)$$

s.t.

$$g_1(\mathbf{P}^S, \mathbf{P}^T) \leq \varepsilon$$

where \mathbf{P}^S and \mathbf{P}^T are B-spline control points matrices of part surfaces from previous and current generations with dimension of $(n_1^S + 1) \times (n_2^S + 1)$ and $(n_1^T + 1) \times (n_2^T + 1)$ correspondingly. $S \cdot$ is B-spline surface definition in Eq. (2.2). g_1 is the general distance (mutual distance) of the two B-spline surfaces. And ε is the maximum

registration error. The mathematical goal of the registration is to find a mapping function by moving the lattice points $\Delta\Phi_{i,j,k}$ to warp the FFD volume space V_S to the volume space V_T , so that the mutual distance between the transformed part surface from previous generation and the part surface of current generation is minimized. For the details of the derivation, refer to Section 2.2.

3.3.2. Overview of the Strain Increment Method

The strain increment method can be explained as follows: since the strain distribution on the existing part is known, if the incremental strain related to the part-to-part mapping can be estimated, the final strain distribution can then be predicted by superposition of both strains. In order to predict the strain from geometry morphing, three assumptions need to be made:

- 1) Material of the new part is the same as that of the existing part. This ensures that the strain and stress rely only on the deformed geometry, but not influenced by material properties;
- 2) The new part design is “similar” to the existing part and the strain paths for forming the new part are similar to that when forming the existing one;
- 3) Strain increment from geometry morphing is defined on the middle surface of the shell, i.e. only membrane strain is considered.

The strain increment method is summarized in the following steps:

- 1) *Mapping of the existing finite element mesh onto the part geometry*: This is the coordinate mapping of finite element mesh in global Cartesian coordinate onto the geometry in the local coordinate, so that in the

following steps of part-to-part mapping, the increment strain can be estimated and superimposed onto the strain distribution of the existing part.

- 2) *Incorporation of a bending energy function and a strain gradient penalty term into part-to-part mapping Eq. (3.1)*: There is no material properties associated to the geometric morphing. Thus, the strain estimation needs to be controlled by a bending energy function and a penalty term to ensure the physical feasibility.
- 3) *Extraction of strain increment from morphing*: The final strain increment is calculated from the displacement field generated by the morphing process and superimposed to the original strain to estimate the strain distribution on the new part. With this strain distribution, further criteria such as strain-based FLD can be used to detect formability.

3.3.3. Mapping of FE Mesh to Geometry

The mapping of existing finite element mesh consists of two parts: 1) Coordinate mapping from global Cartesian coordinate to local (knot) coordinate between 0 and 1; 2) Element connectivity matrix from the old node numbering scheme to new node numbering scheme. In the coordinate mapping, for 2D beam element, it is equivalent to map the nodes into knot vectors U of an NURBS curve (Figure 3.1) defined in Eq. (3.2).

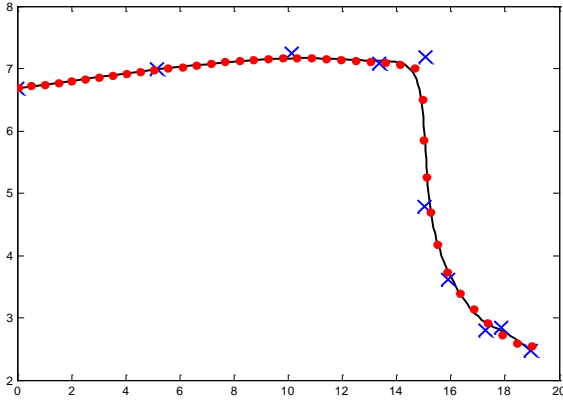


Figure 3.1 Mapping of finite element nodes (dots) on to geometry (crosses are B-spline control points)

$$\begin{aligned}
 u_{node,k} &= f X_k(x, y) \\
 X_k(x, y) &= \sum_{i=0}^n R_{i,p}(u_{node,k}) P_i
 \end{aligned} \tag{3.2}$$

where X_k is the Cartesian coordinate of node k , $R_{i,p}$ is the NURBS basis function of degrees of freedom p , and $P = [P_0 \ P_1 \ \dots \ P_n]$ are the $n+1$ control points (CPs).

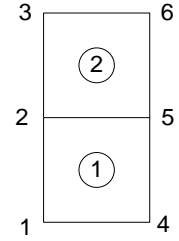
For 3D shell element, a matrix mapping needs to be setup in both U and V directions as defined in Eq. (3.3).

$$\begin{aligned}
 \begin{bmatrix} u_{node,k} & v_{node,k} \end{bmatrix} &= f_{3D} X_k(x, y, z) \\
 X_k(x, y, z) &= \sum_{i=0}^{n_1} \sum_{j=0}^{n_2} R_{i,p}(u_{node}) R_{j,q}(v_{node}) P_{i,j}
 \end{aligned} \tag{3.3}$$

where X_k is the Cartesian coordinate of node k , $R_{i,p}(u)$ and $R_{j,q}(v)$ are the NURBS basis functions of degrees of freedom p and q respectively, and $P_{i,j}$ is the set of control points in matrix form $(n_1 + 1) \times (n_2 + 1)$.

Table 3.1 Element connectivity matrix

Element Number	Local Node 1	Local Node 2	Local Node 3	Local Node 4
1	1	4	5	2
2	2	5	6	3
....				



Element connectivity matrix has the data structure in Table 3.1, where the first column is the element number with the node numbers in subsequent columns. The nodes and their sequence help determine the normal of the shell surface and the local coordinates in calculating the shape functions. Thus, the element connectivity matrix should be the same as that of the existing part.

With the mapping from FE nodes and mesh to geometry being available, the new locations of these nodes can be determined once the part-to-part mapping (movement of lattice point in FFD) is solved. Then, the displacement field as well as the related strain increment can be further solved based on finite element theories.

3.3.4. Strain Increment from Displacement

With the local knot coordinate of each node available, the displacement based on FFD can be obtained combining Eqs. (2.2) and (2.9). In a 2D case, equivalent strain field can be predicted based on “length of the line” by calculating the length of the line segment connecting each pair of nodes. The true strain is obtained by its definition (Figure 3.2),

$$\varepsilon_i = \ln \frac{l_i}{l_i^0} \quad (3.4)$$

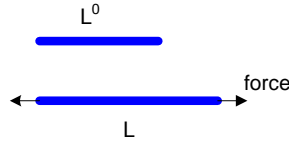


Figure 3.2 Strain prediction in 2D by “length of the line”

In the 3D case, finite element theories of shell element are applied. First, the properties of shell element need to be determined, such as, the lamina (local) coordinate q , and the fiber (thickness) direction ξ (Figure 3.3).

$$\mathbf{q} = [q_{ij}] = [e_1^l \quad e_2^l \quad e_3^l]^T \quad (3.5)$$

where,

$$e_3^l = \frac{e_\xi \times e_\eta}{\|e_\xi \times e_\eta\|}$$

$$e_1^l = \frac{\sqrt{2}}{2} (e_\alpha - e_\beta)$$

$$e_2^l = \frac{\sqrt{2}}{2} (e_\alpha + e_\beta)$$

and,

$$e_\alpha = \frac{1}{2} \frac{(e_\xi + e_\eta)}{\left\| \frac{1}{2} (e_\xi + e_\eta) \right\|}, \quad e_\beta = \frac{e_3 \times e_\alpha}{\|e_3 \times e_\alpha\|}$$

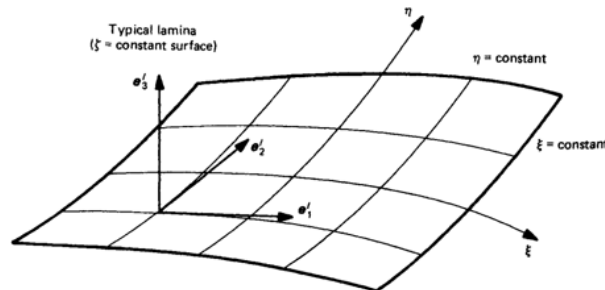


Figure 3.3 Lamina coordinate and fiber direction in a shell element [Hughes, 2000]

The calculation of strain is from the gradient of displacement obtained from the

morphing of all the nodes. Using the finite element theory, the displacement gradient has the form of Eq. (3.6) [Hughes, 2000].

$$\begin{aligned} \frac{\partial u_i^l}{\partial x_j^l} &= \sum_{m=1}^3 q_{im} \frac{\partial u_m}{\partial x_j^l} \\ &= \sum_{m=1}^3 q_{im} \sum_{a=1}^{n_{en}} \left(\frac{\partial u_m}{\partial x_j^l} \bar{u}_{am} + \frac{\partial N_a z_a}{\partial x_j^l} \theta_{a2} - \theta_{a1} \right) \end{aligned} \quad (3.6)$$

where, N_a is the shape function of shell element, $n_{en} = 4$ for a 3D shell, \bar{u}_a is the displacement of each of 4 nodes in a shell element, and z_a is the thickness of shell,

and $\begin{pmatrix} \theta_{a1} \\ \theta_{a2} \end{pmatrix}$ are the rotation of fiber.

In a matrix form, the strain-displacement matrix \mathbf{B} is calculated based on the derivatives of the shape functions of the shell element. Because there is no rotation in the thickness direction by the membrane assumption, \mathbf{B} has the form of:

$$B_a = \begin{bmatrix} b_1^u & b_1^\theta \\ b_2^u & b_2^\theta \\ b_3^u & b_3^\theta \\ \dots & \dots \\ b_4^u & b_4^\theta \\ b_5^u & b_5^\theta \end{bmatrix} \quad (3.7)$$

where,

$$\begin{aligned} b_{1m}^u &= q_{1m} \frac{\partial N_a}{\partial x_1^l} \\ b_{2m}^u &= q_{2m} \frac{\partial N_a}{\partial x_2^l} \\ b_{3m}^u &= q_{1m} \frac{\partial N_a}{\partial x_2^l} + q_{2m} \frac{\partial N_a}{\partial x_1^l} \end{aligned}$$

$$\mathbf{b}_{4m}^u = \mathbf{q}_{2m} \frac{\partial N_a}{\partial x_3^l} + \mathbf{q}_{3m} \frac{\partial N_a}{\partial x_2^l}$$

$$\mathbf{b}_{5m}^u = \mathbf{q}_{3m} \frac{\partial N_a}{\partial x_1^l} + \mathbf{q}_{1m} \frac{\partial N_a}{\partial x_3^l}$$

Finally, strain vectors can be calculated by,

$$\tilde{\boldsymbol{\varepsilon}} = \sum_{a=1}^{n_{en}} \mathbf{B}_a \begin{Bmatrix} \mathbf{u}_a \\ \theta_{a1} \\ \theta_{a2} \end{Bmatrix} = \sum_{a=1}^{n_{en}} \mathbf{B}_a \begin{Bmatrix} \bar{\mathbf{u}}_a \\ 0 \\ 0 \end{Bmatrix} \quad (3.8)$$

3.3.5. Bending Energy and Strain Gradient Functions

The strain predicted directly from geometric morphing (3.1) may not have physical feasibility since there is no material properties related to the geometric morphing process. And solving the displacement field of the nodes using part-to-part mapping is different from finite element theory in which the elastic/plastic constitutive laws are satisfied. Therefore a functional morphing with physical feasibility during geometric morphing is needed. In order to achieve morphing related physical feasibility, two conditions are necessary during the geometric morphing: 1) Minimization of bending energy associated with free-form deformation volume, and 2) Minimization of the strain gradient on the mapped mesh.

A bending energy function J is introduced to the objective function (3.1) to minimize the bending energy of the whole FFD volume. This bending energy function is derived from the strain energy associated with a small deflection of a thin plate [Ventsel, 2001]. It has been adopted for regularization of problems involving discontinuities [Terzopoulos, 1986; Sarraga, 2004].

$$J = \int L(\Delta T) dudvdw \quad (3.9)$$

where,

$$L(\Delta T) = \left(\frac{\partial^2 \Delta T}{\partial u^2} \right)^2 + \left(\frac{\partial^2 \Delta T}{\partial v^2} \right)^2 + \left(\frac{\partial^2 \Delta T}{\partial w^2} \right)^2 + 2\nu \left[\frac{\partial^2 \Delta T}{\partial u^2} \cdot \frac{\partial^2 \Delta T}{\partial v^2} + \frac{\partial^2 \Delta T}{\partial v^2} \cdot \frac{\partial^2 \Delta T}{\partial w^2} + \frac{\partial^2 \Delta T}{\partial w^2} \cdot \frac{\partial^2 \Delta T}{\partial u^2} \right] \\ + 2(1-\nu) \left[\left(\frac{\partial^2 \Delta T}{\partial u \partial v} \right)^2 + \left(\frac{\partial^2 \Delta T}{\partial v \partial w} \right)^2 + \left(\frac{\partial^2 \Delta T}{\partial w \partial u} \right)^2 \right] \\ \Delta T(x, y, z) = \sum_{i=0}^3 \sum_{j=0}^3 \sum_{k=0}^3 B_i(u) B_j(v) B_k(w) \Delta \Phi_{i,j,k}$$

where ν is the Poisson's ratio of the material. In this study, only design surfaces of products are available and only membrane effect is considered. Therefore ν is chosen to be 0.5 (incompressible material).

By including the bending energy function (3.9), the optimization problem of (3.1) is thus equivalent to the Principle of Minimum Potential Energy, where U is the strain energy stored in an elastic body and the external work W is defined by the loading condition. Π is the total potential energy in the system. Thus, Eq. (3.10) can be written as Eq. (3.11) when the total potential energy of a given system has a minimum. The Principle of Minimum Potential Energy states that considering the small-deflection theory of an elastic body, the potential energy is a minimum in an equilibrium state.

$$\Pi = U + W = \int_V \sigma : \varepsilon \, dV - \left[\int_{S_i} u^T f_i \, dV + \int_V u^T f_b \, dV \right] \quad (3.10)$$

$$\delta \Pi = 0 = \delta U + \delta W \quad (3.11)$$

where σ and ε are body stress and strain. u is the vector of displacement. f_b and f_i are body force and surface load acting on the volume and boundary S_i correspondingly.

In this study on sheet metal parts from different generations, since only geometries are considered and the materials of the parts are assumed to be the same, U can be regarded as the bending energy function defined in (3.9). W is equivalent to the

objective function in (3.1) by satisfying the “pre-scribed boundary” where the general distance between the parts is minimized. Thus, the solution of optimizing the problem with including the bending energy function will approximate the equilibrium state.

Minimization of the bending energy related to the whole volume space will lead to a feasible solution. However, sometimes the solved strain distribution is not uniform within the part. Therefore, condition 2 focuses locally on the strain distribution of the part, which is satisfied by introducing a penalty term (3.12) which defines the summation of strain gradient in all directions:

Let ε^j denote the strain associated with element number j ,

$$G = \sum_{j=1}^{n_{ee}} \sum_{i=1}^{n_{sd}} \left(\nabla \varepsilon_{ii}^j \right)^2 = \sum_{j=1}^{n_{ee}} \sum_{i=1}^{n_{sd}} \left(\frac{\partial \varepsilon_{ii}^j}{\partial x_i} \right)^2 \quad (3.12)$$

where n_{sd} is the dimension and n_{ee} is the total number of elements. With such gradient term, no sharp changes in the strain of adjacent elements are allowed during geometric morphing but resulting in much smoother increase or decrease.

Integrating (3.1), (3.9) and (3.12), the final optimization problem (3.13) for the functional morphing between part surfaces is defined by linear combinations of general distance from registration, bending energy function and strain gradient.

$$\mathbf{Min}_{\Delta\Phi} (1 - \alpha - \beta) g_1(P^S, P^T) + \alpha \cdot J + \beta \cdot G \quad (3.13)$$

s.t.

$$g_1(P^S, P^T) \leq \varepsilon$$

$$J = \int L(\Delta T) dudvdw$$

$$G = \sum_{j=1}^{n_{ee}} \left(\nabla \varepsilon_{ii}^j \right)^2 = \sum_{j=1}^{n_{ee}} \sum_{i=1}^{n_{sd}} \left(\frac{\partial \varepsilon_{ii}^j}{\partial x_i} \right)^2$$

where,

$$S(\mathbf{P}) = \sum_{i=0}^{n_1} \sum_{j=0}^{n_2} N_{i,p}(u) N_{j,q}(v) P_{i,j}$$

$$T(x, y, z) = \sum_{i=0}^3 \sum_{j=0}^3 \sum_{k=0}^3 B_i(u) B_j(v) B_k(w) \Phi_{i,j,k}^{(0)} + \Delta \Phi_{i,j,k}$$

$$\mathbf{P}^S = T^{(0)}(x, y, z) = \sum_{i=0}^3 \sum_{j=0}^3 \sum_{k=0}^3 B_i(u) B_j(v) B_k(w) \Phi_{i,j,k}^{(0)}$$

$$L(\Delta T) = \left(\frac{\partial^2 \Delta T}{\partial u^2} \right)^2 + \left(\frac{\partial^2 \Delta T}{\partial v^2} \right)^2 + \left(\frac{\partial^2 \Delta T}{\partial w^2} \right)^2 + \left[\left(\frac{\partial^2 \Delta T}{\partial u \partial v} \right)^2 + \left(\frac{\partial^2 \Delta T}{\partial v \partial w} \right)^2 + \left(\frac{\partial^2 \Delta T}{\partial w \partial u} \right)^2 \right] \\ + \left[\frac{\partial^2 \Delta T}{\partial u^2} \cdot \frac{\partial^2 \Delta T}{\partial v^2} + \frac{\partial^2 \Delta T}{\partial v^2} \cdot \frac{\partial^2 \Delta T}{\partial w^2} + \frac{\partial^2 \Delta T}{\partial w^2} \cdot \frac{\partial^2 \Delta T}{\partial u^2} \right]$$

where α and β are weights valued between 0 and 1, representing trade-offs among the correspondence, the stored bending energy in FFD volume and strain gradient in the part surface. Newton-Raphson numerical method is applied to solving the problem. After solving the mapping functions between existing part and new part, the strain increment can be obtained from Eqs. (3.4)-(3.8). This strain increment is then superposed to the strain distribution of the existing part. And the new strain will help predict the formability using strain-based criteria.

3.4. CASE STUDY

3.4.1. 2D U-shaped Channel Stamping

A 2D U-shaped channel case study similar to Section 2.3.1 has been conducted to demonstrate the strain increment method. A concave feature (Figure 3.4(C)) is added into the original part shape (Figure 3.4 (B)). Both ends of the blank are fixed to prevent material from flowing into the die freely (Figure 3.4 (A)). The purpose of the study is to generate a new die face to produce the concave feature in the new part and compare the

predictions of the strain distribution from both strain increment method and FEA.

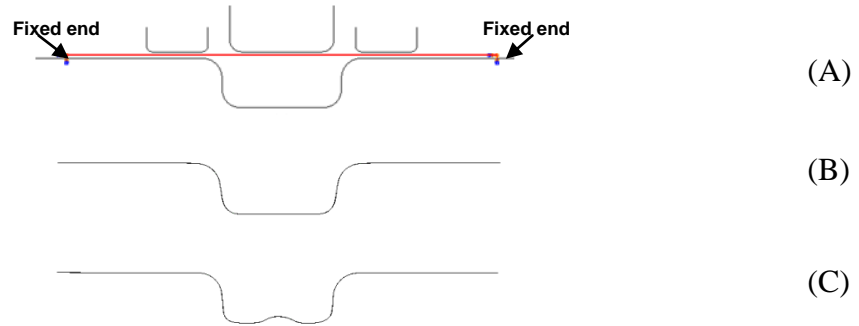


Figure 3.4 2D U-shaped channel case study: (A) existing die and boundary conditions; (B) shape of the existing part; (C) shape of the new part.

3.4.2. Generation of New Die Surface

A 20 CPs NURBS is used to represent the surface of the part. Finite element mesh is mapped to the geometry shown in Figure 3.5.

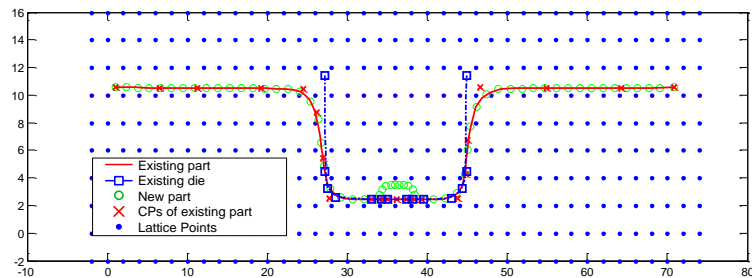


Figure 3.5 Mapping of finite element mesh onto geometry

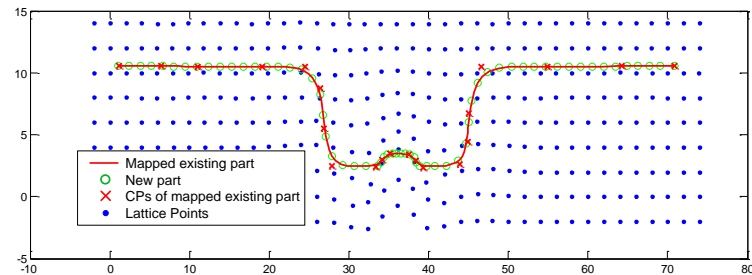


Figure 3.6 Part-to-part mapping solved from (3.13)

The part-to-part mapping function is obtained by functional morphing using Eq. (3.13) with including both bending energy function and strain gradient penalty. The

strain distribution is then calculated and superimposed to the original strain from the existing part. The linear combination coefficients α and β are chosen to be 0.02 and 0.05 correspondingly. Figure 3.6 shows the mapping between the existing part and the new part. By close inspection on the movements of all LPs, the whole space is squeezed upward in the middle to generate the concave shape. Such deformation of the volume space will result in a small bending energy in order to achieve the concave on the bottom.

3.4.3. Strain Prediction by Strain Increment Method

Both the strain increment method and finite element analysis are used to calculate the strain distribution of the new part. Strain distributions of the existing part and the new part calculated from FEA are shown in Figure 3.7. With the concave feature, there are two peaks on the walls of the concave because the material on the walls of the concave is stretched.

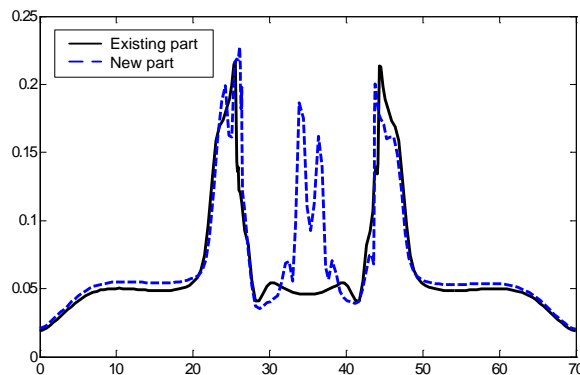


Figure 3.7 Strain prediction on the existing and new parts by FEA

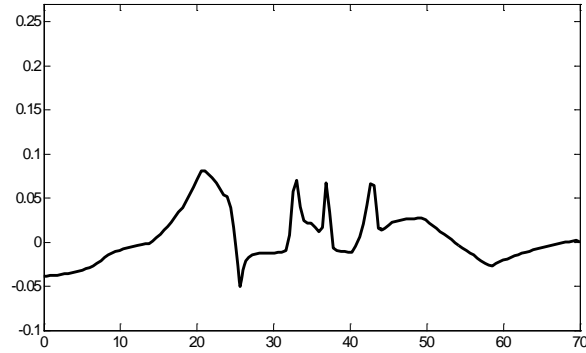


Figure 3.8 Strain increment

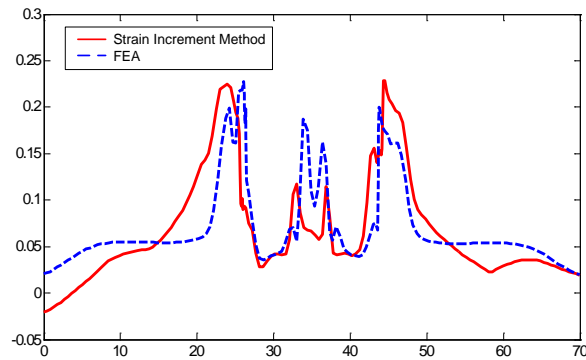


Figure 3.9 Strain prediction by FEA and strain increment method

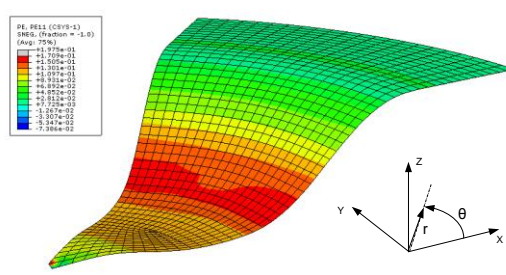
The strain increment calculated from the strain increment method is shown in Figure 3.8. Similar peaks are found near the walls. Combining both results, the comparison of strain increment method and FEA is shown in Figure 3.9. It is seen that, the strain prediction from the strain increment method without having the new die shape is well compared with the strain predicted from FEA. This strain distribution can be further used in formability analysis.

3.4.4. 3D Case Study on Cup Drawing

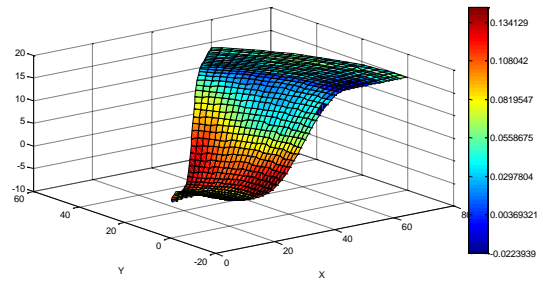
The same cup drawing case study as in Section 2.3.2 is conducted to demonstrate the strain increment method in 3D. The new part shape is modified from the original part shape by adding an increased stamping depth and a concave bottom.

Both the strain increment method and finite element analysis are used to calculate

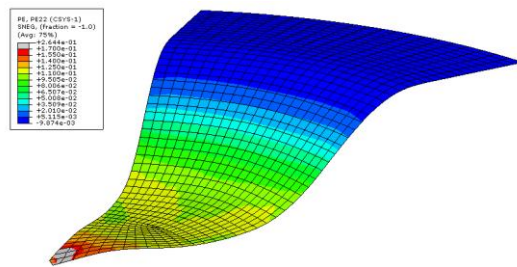
the strain distribution of the new part. Aluminum alloy 6061 has been used for simulation. The plastic strain distributions (circumferential and radial directions in cylindrical coordinate, and in-plane maximum principal) of the new part are shown in Figure 3.10. Both methods are capable to estimate the strain distributions. However, the strain increment method can be applied without the knowledge of the new die face and it is more convenient in the product design stage to quickly estimate the formability a new part design.



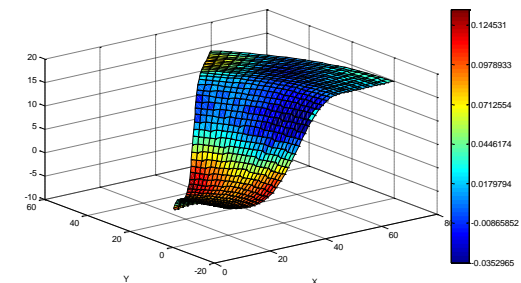
(A) Plastic strain in the circumferential direction from FEA



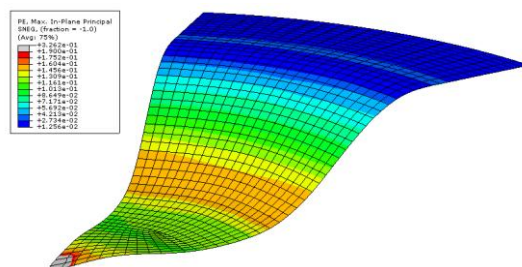
(B) Plastic strain in the circumferential direction from strain increment method



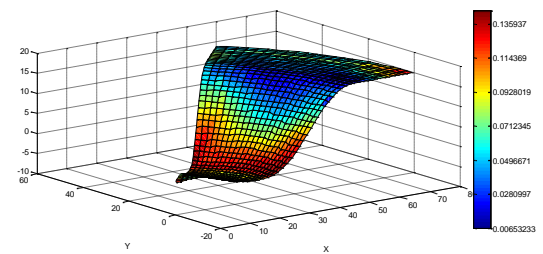
(C) Plastic strain in the radial direction from FEA



(D) Plastic strain in the radial direction from strain increment method

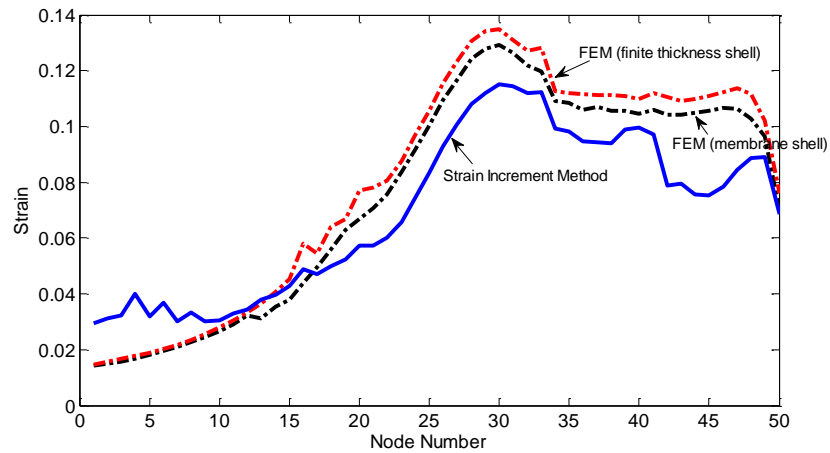


(E) Plastic strain of maximum in-plane principal from FEA

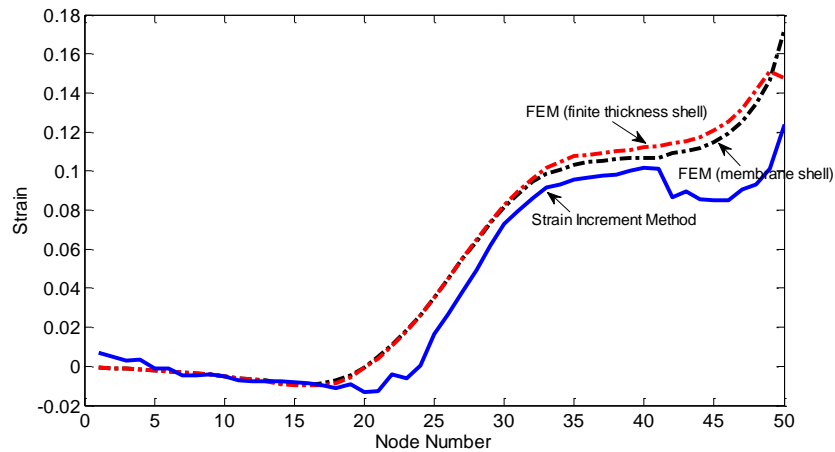


(F) Plastic strain of maximum in-plane principal from strain increment method

Figure 3.10 Strain prediction on the existing and new parts by FEA



(A) Radial strain



(B) Circumferential strain

Figure 3.11 Strains from edge to center of the new part

The strain values are plotted from the edge of the part to the center in Figure 3.11 to compare the results from strain increment method and finite element analyses using both membrane and finite thickness shell elements. It is seen that,

- 1) The strain increment method is able to capture the strain distribution on the new part without having the new die shape. The estimated strain distribution can be further used in formability analysis.
- 2) The algorithms assume strain path similarity. However, in this study, such

similarity exists only on the side wall and on the concave bottom of the cup (except the wall area). Therefore, in regions where there exist strain path difference, the prediction from the strain increment method has more error compared with other regions.

- 3) Discrepancy exists between the predicted strain from strain increment method and that from FEA. Such discrepancy is mainly from three sources: (i) while it is the attempt to consider material/process information in functional morphing, such consideration is still not complete in the functional morphing algorithms, such as strain path history; (ii) different methodologies are used to approach equilibrium state. In finite element analysis, the equilibrium is satisfied during each iteration governed by constitutive equations, but in the strain increment method, it is approximated by minimizing the objective function; (iii) membrane shell ignores the strain distribution in the thickness direction. The difference in strain distribution using the membrane shell and the finite thickness shell is shown in Figure 3.11.

3.5. CONCLUSION

Functional morphing enables fast die development through sequential steps of part-to-part mapping, die-to-die morphing, and finite element verification. Based on the die face morphing algorithm, a strain increment method has been introduced to quickly predict the strain and evaluate the formability for a new generation of part. This method includes mapping of finite element mesh from existing part to the geometry, calculation of strain using finite element theories, and both bending energy and strain gradient penalty terms in solving the functional morphing based part-to-part mapping

function. By superposition of the strain increment to the original strain distribution from the existing part, the strain field on the new part can be estimated without the knowledge of the new die shape. Such strain field can be further used to analyze part formability. Case studies on a 2D U-shaped channel and a 3D cup drawing demonstrate the strain increment method and the predicted strain is compared with the FE simulations in which the new die face is generated by the evolutionary die face morphing method. Results show that strain increment method is able to capture the strain distribution on the new part.

Since the strain increment method does not require the knowledge on new die surface, such formability assessment can be used as an early feasibility assessment of the new part design. Therefore, it is beneficial to both design and DFE in reducing the design/manufacturing iterations in stamping development.

REFERENCES

- Chen, F. K. and Chiang, B. H., (1998), "Three-Dimensional Finite Element Analysis for the Stamping of a Motorcycle Oil Tank", *ASME Transactions: Journal of Manufacturing Science and Engineering*, Vol. 120, pp. 770-773.
- Chen, L. L., Wang, G. F., Hsiao, K. A. and Liang, J., (2003), "Affective Product Shapes through Image Morphing", *Proceedings of the International Conference on Designing Pleasurable Products and Interfaces*, pp. 11-16.
- Chung, K. and Richmond, O., (1992), "Ideal forming I: Homogeneous deformation with minimum plastic work", *International Journal of Mechanical Sciences*, Vol. 34, pp. 575-591.
- Chung, K. and Richmond, O., (1992), "Ideal forming II: Sheet forming with optimum deformation", *International Journal of Mechanical Sciences*, Vol. 34, pp. 617-633.
- Chung, K. and Richmond, O., (1994), "Mechanics of Ideal Forming", *Journal of Applied Mechanics*, Vol. 61, pp. 176-181.

- Chung, K., Barlat, F., Brem, J. C., Lege, D. J. and Richmond, O., (1997), "Blank Shape Design for a Planar Anisotropic Sheet Based on Ideal Forming Design Theory and FEM Analysis", *International Journal of Mechanical Sciences*, Vol. 39 (1), pp. 105-120.
- Guo, Y. Q., Batoz, J. L., Detraux, J. M. and Duroux, P., (1990), "Finite Element Procedures for Strain Estimations of Sheet Metal Forming Parts", *International Journal for Numerical Methods in Engineering*, Vol. 30 (8), pp. 1385-1401.
- Guo, Y. Q., Batoz, J. L., Naceur, H., Bouabdallah, S., Mercier, F. and Barlet, O., (2000), "Recent Developments on the Analysis and Optimum Design of Sheet Metal Forming Parts Using a Simplified Inverse Approach", *Computers and Structures*, Vol. 78 (1), pp. 133-148.
- Hong, D., Fadel, G. M. and Blouin, V. Y., (2006), "Vehicle Component Layout with Shape Morphing - An Initial Study", *Proceedings of 2006 ASME International Design Engineering Technical Conferences and Computers and Information In Engineering Conference, DETC 2006*.
- Hughes, T., (2000), "The Finite Element Method: Linear Static and Dynamic Finite Element Analysis", Dover Publications Inc., New York.
- Kobayashi, S., Oh, S. and Altan, T., (1989), "Metal Forming and the Finite-Element Method", Oxford University Press.
- Lan, J., Dong, X. and Li, Z., (2005), "Inverse Finite Element Approach and Its Application in Sheet Metal Forming", *Journal of Materials Processing Technology*, Vol. 170 (3), pp. 624-631.
- Lin, G., Li, J., Hu, S. J. and Cai, W., (2007), "A Computational Response Surface Study of Three-Dimensional Aluminum Hemming Using Solid-to-Shell Mapping", *Transactions of the ASME: Journal of Manufacturing Science and Engineering*, Vol. 129, pp. 360-368.
- Naceur, H., Guo, Y. Q. and Batoz, J. L., (2004), "Blank Optimization in Sheet Metal Forming Using an Evolutionary Algorithm", *Journal of Materials Processing Technology*, Vol. 151 (1-3), pp. 183-191.
- Ryou, H., Chung, K., Yoon, J. W., Han, C. K., Youn, J. R. and Kang, T. J., (2005), "Incorporation of Sheet-Forming Effects in Crash Simulations Using Ideal Forming Theory and Hybrid Membrane and Shell Method", *ASME Transactions: Journal of Manufacturing Science and Engineering*, Vol. 127 (1), pp. 182-192.
- Sabourin, F., Morestin, F. and Brunet, M., (2004), "Sheet Forming with a Specific Inverse Approach for a Further Springback Analysis", *AIP Conference Proceedings*, Vol. 712, pp. 832-837.

- Saran, M. J., Schedin, E., Samuelsson, A., Melander, A. and Gustafsson, C., (1990), "Numerical and Experimental Investigations of Deep Drawing of Metal Sheets", *Journal of Engineering for Industry*, Vol. 112, pp. 272-277.
- Sarraga, R., (2004), "Modifying CAD/CAM Surfaces According to Displacements Prescribed at a Finite Set of Points", *Computer Aided Design*, Vol. 36, pp. 343-349.
- Sederberg, T. and Parry, S., (1986), "Free-Form Deformation of Solid Geometric Models", *Computer Graphics*, Vol. 20, pp. 151-160.
- Terzopoulos, D., (1986), "Regularization of Inverse Visual Problems Involving Discontinuities", *IEEE Transactions on Pattern Analysis and Machine Intelligence*, Vol. 8 (4), pp. 413-424.
- Ventsel, E. and Krauthammer, T., (2001), "Thin Plates and Shells: Theory, Analysis, and Applications", Marcel Dekker, New York.
- Zhou, L., Hu, S. J., Lin, G. and Stoughton, T.B., (2009), "Evolutionary Stamping Die Development Using Morphing Technology", *Transactions of the NAMRI/SME*, Vol. 37.

CHAPTER 4

FUNCTIONAL MORPHING IN MULTI-STAGE MANUFACTURING AND ITS APPLICATIONS IN HIGH-DEFINITION METROLOGY BASED PROCESS CONTROL

ABSTRACT

In multi-stage manufacturing processes equipped with high-definition metrology (HDM), part shapes can be observed to morph throughout the machining stages in multiple deformation scales, which is caused by the interaction between machining stages and physical attributes of the parts, as defined by *functional morphing*. Functional morphing characterizes the dependence of surface characteristics at downstream stages on surface characteristics from upstream stages. Conventional methodology to study the inter-stage relationship focuses on variation propagation of discrete key product characteristics or surface vectors and has limitations in analyzing HDM data for complex shape changes. This chapter investigates the functional morphing and explores its applications in improving variation reduction strategy. A functional free form deformation approach is developed to extract mapping functions between manufacturing stages. The obtained mapping functions enable multi-scale

Contents of this chapter are to be submitted to *IEEE Transactions: Automation Science and Engineering*.

variation propagation analysis and intermediate stage process monitoring. It also allows for accurate inter-stage adjustment that introduces shape deformation upstream to compensate for the end-of-line errors. The developed monitoring and adjustment algorithms are demonstrated via a case study of a two-stage machining process. Other application such as process tolerance design is also discussed.

4.1. INTRODUCTION

High-definition metrology (HDM), a new surface inspection technology with high resolution, has become a key enabler of high-precision manufacturing. Figure 4.1 shows a scanned surface on a V-8 engine head, where the color indicates the height measurement (μm). It can be seen that the surface is of a “bowl” shape form. Meanwhile, features in small scale related to tooling conditions (e.g., tool mark) are also observed. When HDM is applied to a multistage manufacturing process, the changes of part surfaces from stage to stage in a complex manner can be analyzed as morphing. The inter-stage changes may occur at multiple scales: global shape, local defects with different sizes, and waviness. Figure 1.3 shows a two-stage machining process that mills the part top surface (Op1) followed by a drilling operation on its side (Op2). It can be seen from Figure 1.3(C, D) that surface exiting Op2 differs from Op1 in both global shape and local defect (a small bump in the middle).

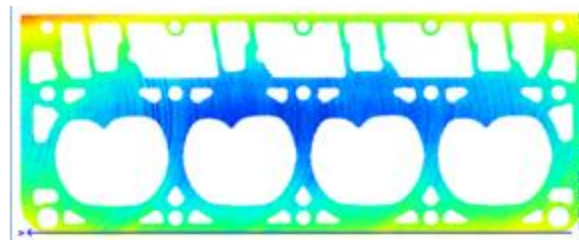


Figure 4.1 V-8 engine head measured by HDM device

In a multistage machining process, the part surface change includes shape, waviness, and key product characteristics that reflect the inter-stage interaction of given process settings and part physical properties such as mass density, casting pore distribution, and mechanical properties. For instance, Figure 1.3 describes the change from 2 operations: milling and drilling. Such change is the result of the joint effect of the geometrical shape due to the cutter path and the mechanical/materials interactions of cutting force, deformation and springback. Therefore, *functional morphing* is needed to describe the part feature change between stages caused by the process conditions and part physical properties, instead of using pure geometric morphing.

In computer graphics, morphing patterns are captured by mathematical transformation which maps any point on the source object to the corresponding point on the target object. The most commonly used transformation techniques include affine transformation and quadratic transformation [Hearn and Baker, 1994], Thin Plate Spline (TPS) [Bookstein, 1989], and Free-Form Deformation (FFD) [Sederberg, 1986; Coquillart, 1990]. The affine transformation is usually utilized for rigid body but lacks the degrees of freedom to describe the complex shape changes. Quadratic transformation offers more but still limited degrees of freedom. TPS and FFD are commonly adopted approaches for an accurate characterization of surfaces with global-local feature changes. However, these methods are data-oriented and may yield transformations that are difficult to interpret since no physical insights are provided. For the control of a multistage manufacturing process, it is necessary to extend from the geometry morphing to the *functional morphing*.

Existing research on manufacturing process control focuses on the variation

propagation that investigates the variations accumulated through upstream stages and their impact on current and downstream stages, as reviewed by [Shi, 2006]. This line of research includes multistage variation propagation modeling [Mantripragada and Whitney, 1999; Jin and Shi, 1999; Djurdjanovic and Ni, 2001; Zhou, et al. 2003; Camelio, et al. 2003], model based process fault diagnosis [Ding, et al. 2002; Zhou, et al. 2004], multistage process tolerance design [Huang and Shi, 2003; Ding, et al. 2005], as well as process adjustment with programmable toolings [Wang and Huang, 2007; Zhong, et al. 2009]. Utilizing vectorial surface model [Huang, et al. 2003] or discrete nodes (obtained from CMM scanning or finite element analysis) to represent the surface shape [Camelio, et al. 2003], these methods modeled functional morphing either by engineering knowledge such as rigid body kinematics for rigid parts [Cai, et al. 1996] and finite element analysis for compliant parts [Camelio, et al. 2003], or by data driven approach [Apley and Shi, 2001; Liu, et al. 2008].

The aforementioned approaches used vectorial surface model and vector of low-dimensional scanned data or FEM nodes to represent part surfaces. However, they are not appropriate for HDM data analysis. The vectorial surface model presents limited surface information in that it mainly captures the features with regular shape such as planar or cylindrical. And using FEM nodes could increase the computational load exponentially due to fine meshing. Furthermore, these approaches did not distinguish feature changes in different scales such as global shape, local deformation, or surface waviness and therefore the number of variation sources considered in variation propagation modeling is limited (e.g., cutter's condition and cutting force, variation of material properties). Engineering process models should be used in

conjunction with morphing technology in computer graphics to derive the functional morphing.

This chapter develops functional morphing modeling for process variation propagation analysis in a multistage machining process. Functional morphing models are established based on the morphing technology in computer graphics among part features. The extracted morphing patterns are applied in process control including inter-stage process monitoring and adjustment and process design.

This chapter is organized as follows: Section 4.2 develops functional morphing modeling and extracts morphing pattern based on free-form deformation (FFD), by which the surface variation propagation is derived from HDM data. Section 4.3 presents the detailed algorithms in morphing based process monitoring and control. The proposed algorithms are then demonstrated by a case study in Section 4.4. Conclusions are drawn in Section 4.5.

4.2. MODELING OF SURFACE CHANGES USING FUNCTIONAL MORPHING

Conventional morphing is a mapping between geometries where only pure geometric relationship is considered. Functional morphing incorporates mechanical properties in addition to geometric relationship, so that physical feasibility is satisfied in a geometric mapping process. This section develops functional morphing to model surface changes between stages using feature extraction of HDM data, forward and backward mapping functions, and variation propagation through morphing.

4.2.1. Feature Extraction

Although HDM measurements can provide rich information on different scales of features and the associated process conditions, HDM data may have redundancy and cause unnecessary computational load. Thus, HDM data should be preprocessed to the scale of interest. For example, global flatness is evaluated at a large scale, while waviness or tool mark may require a much smaller scale.

The metrology using laser holographic interferometry produces scattered data for x , y , and z coordinates on a machined surface. For variation control, the primary concern is to analyze height (z) values that are spatially distributed along the x and y directions. One way to extract such feature is to project the scattered HDM data onto rectangular grids through interpolation and extrapolation methods, where the size of the grids determines the scale of study, i.e., coarse grid extracts global scale features (e.g., global flatness), while dense grid extracts small scale features (e.g., tool mark). Figure 4.2 shows an example of using triangle interpolation to obtain surface grids, where z_i 's are scattered data from measurements and z'_i 's are the projected data on grids. The objective is to find an interpolation method A and z' such that,

$$\min_{A, z'} \|Az' - z\|^2 \quad (4.1)$$

where $z = [z_1 \ z_2 \ \dots]^T$ and $z' = [z'_1 \ z'_2 \ \dots]^T$. For detailed procedures, refer to [Keim and Herrmann, 1998].

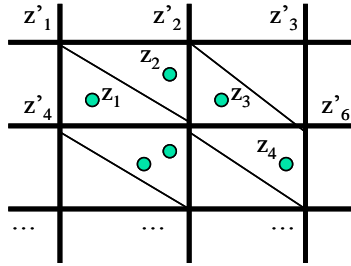


Figure 4.2 Projection of scattered data onto grids

z' can be re-written in a matrix form according to the dimension of the rectangular grids. In the remainder of the chapter, matrix S is introduced to represent the coordinates of surface grids of dimension $(d_1 \times d_2)$.

4.2.2. Functional Morphing for Surfaces

A functional morphing is developed to map the surfaces between manufacturing stages. Two morphing functions are introduced: (1) Forward mapping function transforms the surface from one stage to the next in a forward direction. Thus, if a scanned surface is known at the current stage, the surface at any downstream stage can be estimated. (2) Backward mapping function transforms the surface from one latter stage to a prior stage. The nominal surface at any upstream stage can be estimated if the surface at the final stage is specified.

Forward Mapping Function

Consider a multi-stage manufacturing process including stages labeled from 0 (incoming part) to I (final stage). Assume that the surfaces from stage i and $i+1$ are defined by their surface grids sets S^i and S^{i+1} respectively and $T^{i+1,i}$ is defined as the mapping function from stage i to $i+1$. The goal of forward mapping is to find a $T^{i+1,i}$ so that the difference between S^i and S^{i+1} are minimized.

Both Free-form deformation (FFD) and Thin-plate spline (TPS), which is derived from minimization of bending energy of a thin plate given point constraints, can be used as the morphing method because they have the degrees of freedom to capture complex surface changes. However, FFD has the advantages over TPS as listed in Table 4.1. Therefore, a cubic Free-form Deformation (FFD) has been selected as the morphing method.

Table 4.1 Comparison of Free-Form Deformation and Thin Plate Spline

	Free-form deformation	Thin plate spline
Deformation localization	Each embedded point is defined by adjacent 64 lattice points in FFD volume.	Each basis function or points has global effect on transformation. Local deformation is not available.
HDM compatibility	Measured points are embedded in the FFD volume while variables are the lattice to define the volume. Therefore, FFD is HDM compatible.	Not feasible to constrain each measured point to formulate TPS transformation.

The cubic FFD is defined as,

$$\begin{aligned}
 x \quad y \quad z &= \sum_{l=0}^3 \sum_{m=0}^3 \sum_{n=0}^3 B_l(u) B_m(v) B_n(w) \Phi_{l,m,n} \\
 &= \sum_{l=0}^3 \sum_{m=0}^3 \sum_{n=0}^3 B_l(u) B_m(v) B_n(w) \left[\Phi_{l,m,n}^X \quad \Phi_{l,m,n}^Y \quad \Phi_{l,m,n}^Z \right]
 \end{aligned} \tag{4.2}$$

where (u, v, w) are localized coordinates corresponding to the global coordinates (x, y, z) and B 's are the uniform cubic B-Spline blending functions defined in Eq. (2.6). $\Phi_{i,j,k}$ are the lattice points (LP) defining the FFD volume space.

If S^i has the dimension of $(d_1 \times d_2)$, at the initial stage 0, the local coordinates $(u_a,$

v_a, w_a) of point S_a^0 in S^0 , $a=1\dots d_1 \times d_2$, are determined by (4.3),

$$S_a^0 |_0 = \sum_{l=0}^3 \sum_{m=0}^3 \sum_{n=0}^3 B_l(u_a |_0) B_m(v_a |_0) B_n(w_a |_0) \cdot \Phi_{l,m,n}^0 \quad (4.3)$$

where Φ^0 is the initial FFD volume space. The notation $\bullet|_0$ denotes that \bullet is measured at stage 0. The local coordinates determined at stage 0 are invariant for the morphing over the subsequent stages.

In FFD, new surface is generated by deforming the volume space Φ . Thus, at any stage i , the surface grids S^i can be written as,

$$S_a^i |_0 = \sum_{l=0}^3 \sum_{m=0}^3 \sum_{n=0}^3 B_l(u_a |_0) B_m(v_a |_0) B_n(w_a |_0) \cdot \Phi_{l,m,n}^i \quad (4.4)$$

where Φ^i is the FFD volume space at stage i .

Definition 1: Continuous Forward Mapping

Define $\Delta\Phi^{j,i}$ be the deformation of FFD volume space from stage i to j . Continuous forward mapping states that the volume space at any stage after measurement at stage (i) is determined by the summation of all mapping functions from stage j to i .

$$\Phi^j = \Phi^i + \Delta\Phi^{j,i} = \Phi^i + \Delta\Phi^{i+1,i} + \dots + \Delta\Phi^{j,j-1} \quad (i \leq j) \quad (4.5)$$

Then,

$$\begin{aligned} \hat{S}_a^j |_i = & \sum_{l=0}^3 \sum_{m=0}^3 \sum_{n=0}^3 B_l(u_a |_i) B_m(v_a |_i) B_n(w_a |_i) \\ & \cdot \Phi_{l,m,n}^i + \Delta\Phi_{l,m,n}^{i+1,i} + \dots + \Delta\Phi_{l,m,n}^{j,j-1} \end{aligned}$$

where $\hat{S}_a^j |_i$ is the estimated surface grid matrix at stage i .

An optimization problem (4.6) considering only geometric relationship is

formulated to solve the mapping function $\Delta\Phi^{i+1,i}$ for 2 consecutive stages.

$$\begin{aligned} \mathbf{Min}_{\Delta\Phi^{i+1,i}} \quad & g_1(S^i |_i, S^{i+1} |_i) \\ \text{s.t.} \quad & g_1(S^i |_i, S^{i+1} |_i) \leq \varepsilon \end{aligned} \quad (4.6)$$

where g_1 is a mutual distance function measuring the distance between two surfaces defined by surface grids, and ε is the maximum registration error between the surface grids at stage i and $i+1$.

The solution to (4.6) is not unique, and constraints and penalty functions governed by physical laws are needed to ensure the feasible solution region. In this study, the penalty function is chosen to be bending energy J defined in Eq. (4.7), which is derived from the strain energy associated with a small deflection of a plate [Ventsel and Krauthammer, 2001].

$$J = \int L(\Delta\mathbf{T}) du dv dw \quad (4.7)$$

where,

$$\begin{aligned} L(\Delta\mathbf{T}) = D \cdot & \left\{ \left(\frac{\partial^2 \Delta\mathbf{T}}{\partial u^2} \right)^2 + \left(\frac{\partial^2 \Delta\mathbf{T}}{\partial v^2} \right)^2 + \left(\frac{\partial^2 \Delta\mathbf{T}}{\partial w^2} \right)^2 + 2\nu \left[\frac{\partial^2 \Delta\mathbf{T}}{\partial u^2} \cdot \frac{\partial^2 \Delta\mathbf{T}}{\partial v^2} + \frac{\partial^2 \Delta\mathbf{T}}{\partial v^2} \cdot \frac{\partial^2 \Delta\mathbf{T}}{\partial w^2} + \frac{\partial^2 \Delta\mathbf{T}}{\partial w^2} \cdot \frac{\partial^2 \Delta\mathbf{T}}{\partial u^2} \right] \right. \\ & \left. + 2(1-\nu) \left[\left(\frac{\partial^2 \Delta\mathbf{T}}{\partial u \partial v} \right)^2 + \left(\frac{\partial^2 \Delta\mathbf{T}}{\partial v \partial w} \right)^2 + \left(\frac{\partial^2 \Delta\mathbf{T}}{\partial w \partial u} \right)^2 \right] \right\} \end{aligned}$$

and,

$$\begin{aligned} D(u, v, w) &= \frac{E(u, v, w)h(u, v, w)^3}{12(1-\nu^2)} \\ \Delta\mathbf{T} &= \sum_{l=0}^3 \sum_{m=0}^3 \sum_{n=0}^3 B_l(u)B_m(v)B_n(w)\Delta\Phi_{l,m,n} \end{aligned}$$

where E is the Young's modulus, h is an equivalent thickness function derived from the real part and ν is the Poisson's ratio. Space-varying variable D can characterize heterogeneous properties of parts.

Similar to the bending energy of FFD volume defined in Chapter 3 for strain increment method, the optimization problem (4.6) is also equivalent to the Principle of Minimum Potential Energy in Eq. (4.8) by including the energy term in Eq. (4.7) with extended physical properties. In Eq. (4.8), δU is the change of strain energy stored in an elastic body and the change of external work δW is defined by the loading condition. Π is the total potential energy. The solution to Eq. (4.8) results in an equilibrium state.

$$\delta \Pi = 0 = \delta U + \delta W \quad (4.8)$$

In our study where the material remains the same throughout the manufacturing process, U can be regarded as the bending energy defined in (4.7). W is equivalent to the objective function in (4.6) by satisfying the “pre-scribed boundary” where the mutual distance between the part surfaces is minimized. Thus, the solution to the optimization problem (4.6) combined with (4.7) will approximate the equilibrium state.

Finally, a new optimization problem is formulated in (4.9).

$$\mathbf{Min}_{\Delta \Phi^{i+1,j}} (1-\alpha) g_1(S^i |_i, S^{i+1} |_i) + \alpha \cdot J \quad (4.9)$$

where α is the optimization parameter between 0 and 1, which indicates the trade-off between registration error and stored bending energy inside FFD volume.

Backward mapping function

Similar to the forward mapping which considers the mapping from a previous stage to a latter one, when the desired final surface at stage (I) $S^I |_I$ is specified, the nominal surface shape (or desired surface shape) at any previous stage i can be estimated by using backward mapping.

The backward mapping function can be derived based on the forward mapping function by sharing the same FFD volume space Φ^i ($i = 1 \dots I$) at each stage. Given the

final surface $S^I|_l$, Eq. (4.3) can be used to determine the local coordinates $[u \ v \ w]^T|_l$.

Definition 2: Continuous Backward Mapping

The FFD volume space at any stage is determined by the summation of all mapping functions from stage I to i ($i \leq I$).

$$\Phi^i = \Phi^I + \Delta\Phi^{i,I} = \Phi^I + \Delta\Phi^{I-1,I} + \dots + \Delta\Phi^{i,i+1} \quad (4.10)$$

where $\Delta\Phi^{i,i+1} = -\Delta\Phi^{i+1,i}$

Similarly, at each stage i , the nominal surface shape represented by $\hat{S}^i|_l$ is calculated by,

$$\hat{S}_a^i|_l = \sum_{l=0}^3 \sum_{m=0}^3 \sum_{n=0}^3 B_l(u_a|_l) B_m(v_a|_l) B_n(w_a|_l) \cdot \Phi^I_{l,m,n} - \Delta\Phi^{I,I-1}_{l,m,n} + \dots + \Delta\Phi^{i+1,i}_{l,m,n} \quad (4.11)$$

4.2.3. Morphing Based Multi-stage Variation Modeling

In manufacturing processes, variations can be attributed to many sources, such as fixturing, clamping, tooling conditions, etc. This section investigates the variation propagation of complex surface features through functional morphing.

In functional morphing of manufacturing stages, the volume space Φ^i is fixed at each stage. The local coordinates of each surface grid is invariant throughout the stages. Therefore, it is needed to identify the variation of these local coordinates of surface grids due to process perturbations. The variation of local coordinates of surface grids is then transformed into global coordinate to assess the variation of the surface.

Assume at stage i , there are p_i variation sources. Define the source covariance matrix at stage i as Σ_F^i with dimension $3p_i \times 3p_i$ (in X, Y and Z directions). Also define the sensitivity matrix at stage i from these variation sources to surface grid points as s^i

from Eq.(4.4).

The morphing based variation propagation can be modeled by

$$\begin{aligned}\sigma_{SP}^i &= \sigma_{SP}^{i-1} + \sigma_{SF}^i \\ &= \sigma_{SP}^{i-1} + (J^i)^{-1} \cdot \left[\Sigma_{SF}^i \right] \cdot (J^i)^{-T}\end{aligned}\quad (4.15)$$

where σ_{SP}^i is the accumulated variation up to stage i , $i=1..I$ and at the initial stage $\sigma_{SP}^0 = \mathbf{O}$. The local coordinates of surface grids will follow a multi-normal distribution, i.e.,

$$U^i \sim N \left[\mu_{SP}^i, \left[\sigma_{SP}^i \right] \right] \quad (4.16)$$

where $\left[\mu_{SP}^i \right] = \left[u_{1,1} \quad v_{1,1} \quad w_{1,1} \quad u_{1,2} \quad v_{1,2} \quad w_{1,2} \quad \cdots \quad u_{d_1,d_2} \quad v_{d_1,d_2} \quad w_{d_1,d_2} \right]^T$. Based on the definition of variance, the covariance matrix of the global coordinates of surface grids is,

$$\Sigma_{SP}^i = \begin{bmatrix} v_{1,1} & v_{1,2} & \cdots & v_{1,3(d_1 \times d_2)} \\ & v_{2,2} & & \vdots \\ & & v_{a,a} & \\ \text{symmetric} & & & v_{3(d_1 \times d_2) \times 3(d_1 \times d_2)} \end{bmatrix} \quad (4.17)$$

where the entries to the matrix are calculated by,

$$\begin{aligned}v_{a,a} &= \text{Var}(S_a^i) = E \left[S_a^i \right]^2 - \left[E \left[S_a^i \right] \right]^2 \\ v_{a,b \neq a} &= \text{Cov}(S_a^i, S_b^i) = E \left[S_a^i \cdot S_b^i \right] - E \left[S_a^i \right] \cdot E \left[S_b^i \right] \\ E(S_a^i) &= \sum_{l=0}^3 \sum_{m=0}^3 \sum_{n=0}^3 B_l(u_a |_i) B_m(v_a |_i) B_n(w_a |_i) \cdot \Phi_{l,m,n}^i\end{aligned}$$

Similar methodologies can be derived for the backward mapping, by which tolerance design for the manufacturing process can be performed if the design specification of the final surface is known.

4.3. APPLICATIONS OF FUNCTIONAL MORPHING IN MACHINING PROCESS CONTROL


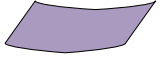
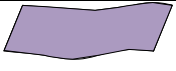

Using the morphing based variation propagation model, this section discusses three potential applications for machining process control including inter-stage process adjustment, process monitoring and tolerance design.

4.3.1. Inter-stage Process Adjustment

Functional morphing can be utilized to conduct an inter-stage process adjustment by introducing deformation upstream to compensate for the end-of-line errors. The artificially introduced deformation can be generated by adjusting process variables such as fixturing, clamping, and machining parameters. The advantage of the inter-stage process adjustment is that the compensation of complex form errors can be allocated onto multiple stages, thus reducing adjustment cost for each stage.

Consider a multi-stage manufacturing system as shown in Table 4.2. Assume that the measurement is conducted at stage i . The optimal strategy should apply adjustments from stage i to I so that the surface at the end stage is as close as to the desired shape $S^I |_I$ with a minimum variance. The formulation is given in Eq. (4.18), where the continuous forward mapping is used to estimate the surface at the final stage. Meanwhile, the objective is obtained similar to the signal-to-noise ratio (SNR) [Taguchi, 1986; Wu and Hamada, 2000] by calculating the inverse of sum square error of surface grids over the sum of their variances.

Table 4.2 Manufacturing system for inter-stage error compensation

	Stage 0	..	Stage i	Stage $i+1$...	Stage I
Shape						
Surface Grids	S^0		S^i	S^{i+1}		S^I
FFD lattice	Φ^0		Φ^i	Φ^{i+1}		Φ^I
Covariance matrix	Σ_F^0		Σ_F^i	Σ_F^{i+1}		Σ_F^I

$$\begin{aligned} \mathbf{Max}_{\lambda_j (i \leq j \leq I)} & 10 \log_{10} \left(\frac{1}{\|\hat{S}^I |_{i} - S^I |_{i}\|^2} \cdot \frac{1}{\text{trace } \hat{\Sigma}_{SP}^I |_{i}} \right) \\ & = -10 \left[2 \cdot \log_{10} \|\hat{S}^I |_{i} - S^I |_{i}\| + \log_{10} \text{trace } \hat{\Sigma}_{SP}^I |_{i} \right] \end{aligned} \quad (4.18)$$

s.t.

$$L_{\lambda_j} \leq \lambda_j \leq U_{\lambda_j} \text{ for all } (i \leq j \leq I)$$

where,

$$\hat{S}_a^I |_{i} = \sum_{l=0}^3 \sum_{m=0}^3 \sum_{n=0}^3 B_l(u_a |_{i} + \sum_{j=i}^I \Delta u_a |_{j}) B_m(v_a |_{i} + \sum_{j=i}^I \Delta v_a |_{j}) B_n(w_a |_{i} + \sum_{j=i}^I \Delta w_a |_{j}) \cdot \Phi^I_{l,m},$$

($a = 1 \dots d_1 \times d_2$, $[\Delta u_a |_{j}, \Delta v_a |_{j}, \Delta w_a |_{j}]$ is change of local coordinates of

surface grids due to the adjustments λ_j with upper and lower limits being

U_{λ_j} and L_{λ_j} , respectively.)

$$\sigma_{SP}^i = \sigma_{SP}^{i-1} + \sigma_{SF}^i = \sigma_{SP}^{i-1} + (J^i)^{-1} \cdot [\Sigma_{SF}^i] \cdot (J^i)^{-T}$$

Σ_{SP}^i is derived based on σ_{SP}^i using Eq. (4.17).

The solution to (4.18) gives the optimal adjustment strategy from the measurement stage i to the end of the manufacturing process.

4.3.2. Backward Morphing Based Process Monitoring

Section 4.3.1 introduces an error compensation strategy to adjust process to improve final surface flatness and reduce its variance. Process monitoring is then needed to ensure process repeatability based on such optimized process adjustment. In process monitoring, backward surface morphing based on the updated process adjustment can be utilized to predict all the surfaces at prior stages to reduce extra measurements. Such process monitoring is illustrated in Figure 4.3.

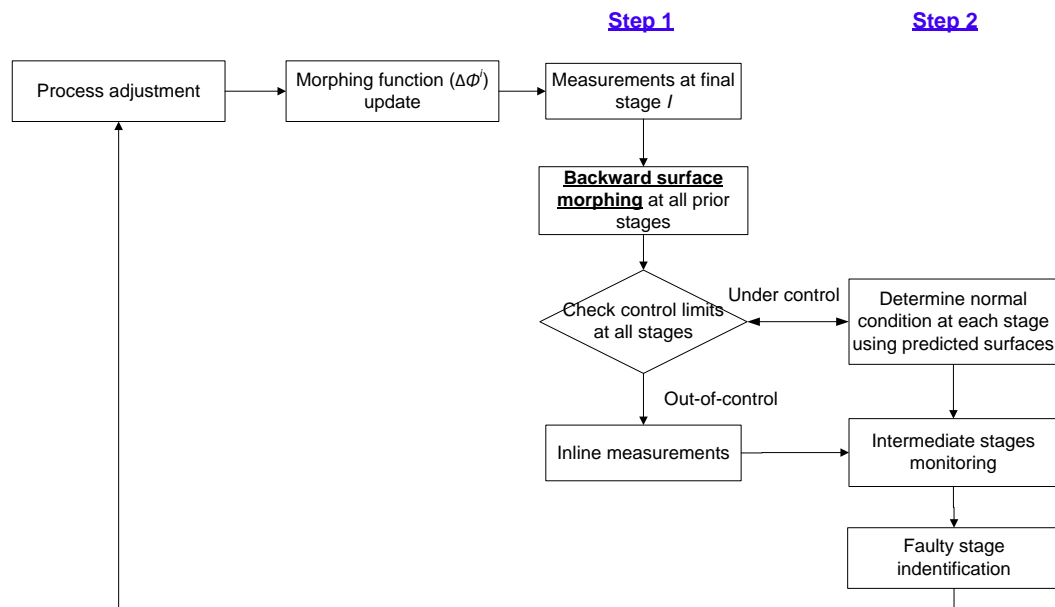


Figure 4.3 Schematic diagram for multi-stage process monitoring

There are 2 major steps in the process monitoring: (1) Surface measurement is taken at the final stage I and backward morphed to all upstream stages from $I-1$ to 0. If all the morphed surfaces including the measured surface at final stage are within the control limits, the process is concluded as “under control”. Then, (2) these measured and predicted surfaces can be used to determine the normal condition at each stage from I to 0 and setup the process control charts at these stages. In the case when

measured surface at final stage and/or some morphed surfaces at prior stages are out-of-control, then inline measurements are taken at these stages and fed into control charts to localize faulty stages. Compared with 100% inspection at all stages, the proposed monitoring strategy requires fewer measurements.

The covariance matrix for the surface grids $\Sigma_{SF}^I | I$ is first determined by a number of measured parts to setup the control limits at the final stage. These surface grids follow a multi-normal distribution $N(\bar{S}^I, \Sigma_{SF}^I)$, where averaged surface \bar{S}^I estimates the mean and multivariate monitoring methods can be applied for statistical process control. Since the monitored surface grids, S^I 's, can be highly spatial correlated, dimension reduction techniques, such as Principal Component Analysis (PCA), can be applied to filter out redundant information and reduce the misdetection rate. Process control charts for intermediate stages can be constructed similarly by estimating the surface grids using backward mapping functions (4.10)-(4.11) if the measured surfaces from final stage I are all under control.

Once an out-of-control is detected at some stage, backward mapping will no longer work since it was established based on normal conditions. Further measurements are needed at prior stages to identify the faulty stage as well as root causes.

4.3.3. Process Tolerance Design

Variation propagation modeling derived using forward morphing (Eq. (4.5)) could improve the tolerance stackup prediction and tolerance allocation that minimizes the tooling cost while ensures the final product dimensional tolerance. Typically, minimizing tooling cost is equivalent to maximizing the sum of process tolerances. Let

Θ denote a vector including n process variables in the multi-stage process

$$\Theta = [\theta_1 \ \theta_2 \ \dots \ \theta_n]^T.$$

$$\begin{aligned} & \mathbf{Max}_{\sigma_{\theta_i}^2} \text{trace}(\Sigma_{\Theta}) \\ & \text{s.t.} \\ & \Sigma_1^I + \Sigma_2^I + \dots + \Sigma_I^I \leq b_1 \\ & 0 \leq \sigma_{\theta_i}^2 \leq b_{i,2} \end{aligned} \tag{4.19}$$

where Σ_{Θ} represents covariance matrix Θ that determines the process variable tolerance; σ_{Θ}^2 is a vector consisting of all the diagonal entries in the matrix Σ_{Θ} ; $\Sigma_1^I + \Sigma_2^I + \dots + \Sigma_I^I$ represents the variances of features that also reflect tolerance stackup, where Σ_i^I derived by Eqs. (4.12) - (4.17) denotes variation introduced at the i th stage accumulated onto the final stage; b_1 gives the specified product feature tolerance and $b_{i,2}$ gives the practical constraint of each tooling variation $\sigma_{\theta_i}^2$. Solution to this problem can follow the procedures in [Huang and Shi, 2003]. Tolerance of process variables θ_i at each stage can then be determined by σ_{θ_i} .

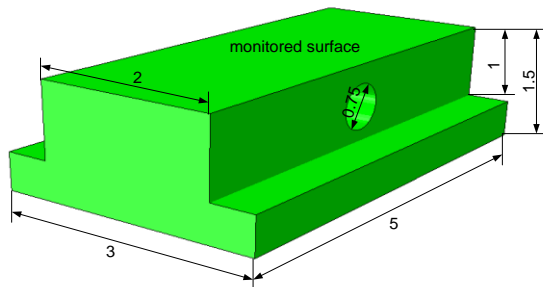
4.4. CASE STUDY

An experimental study is conducted to demonstrate the closed-loop morphing based process control strategy. The experiment is based on the 2-stage manufacturing processes including face milling and drilling (Figure 1.3).

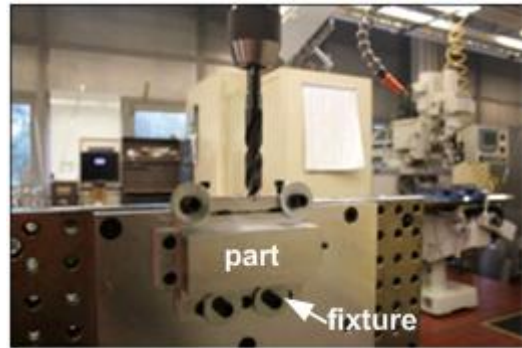
4.4.1. Experimental Setup

A “ \perp ” shape part is chosen for the experiment, the dimension of which is shown in Figure 4.4(A). The material of the part is aluminum alloy 2024, whose mechanical

properties are listed in Table 4.3. For experimental purposes, an adjustable fixture and clamping are designed as shown in Figure 4.4(B). The clamping force is controllable through threads and calibrated using torque wrench, while the fixture height in the Z direction can be adjusted by inserting aluminum foil (0.01” thick). During the drilling process, the whole fixture is mounted on a 90° angle plate, which is attached to the base of the NC machine.



(A) Dimension of the generic part (unit: inch)



(B) Drilling process

Figure 4.4 Experimental setup

Table 4.3 Mechanical properties of Aluminum Alloy 2024

Density ($\times 1000 \text{ kg/m}^3$)	2.77	Elongation (%)	20
Poisson's Ratio	0.33	Hardness (HB500)	47
Elastic Modulus (GPa)	70	Shear Strength (MPa)	125
Tensile Strength (MPa)	185	Fatigue Strength (MPa)	90
Yield Strength (MPa)	76		

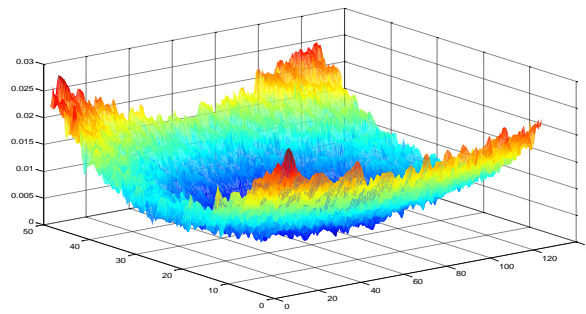
The top surface of the part is monitored and scanned by a laser holographic interferometer after each stage. The following stage and measurement steps are conducted:

- 1) Face mill the top surface and take the initial measurement before releasing the clamping. The measured surface profile is regarded as incoming surface.
- 2) Take the second measurement after releasing the clamping. By releasing the clamping forces, some deformation on the top surface will be recovered depending on the magnitude of the clamping forces.
- 3) Mount the part back to the fixture, drill the side hole (Figure 4.4(B)) and then take the third measurement on the top surface after releasing from fixture. It is expected that localized defect on the top surface will be generated due to drilling.

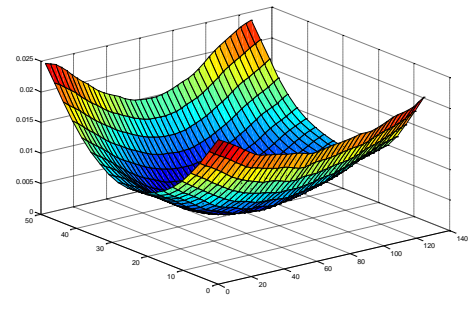
4.4.2. Functional Morphing Between Stages

The forward mapping method in Section 4.2.2 is utilized to establish the functional morphing between stages. Before mapping, the global feature is extracted through triangular interpolation as shown in Figure 4.5. The data dimension is reduced from 150k to 800 points on regularized grids.

Results of the functional morphing are shown in Figure 4.6 for both stages. The coefficient α in the optimization is chosen to be 0.01 which is believed to well incorporate the physical feasibility of each stage. It is seen that, after releasing the clamping forces in the face milling stage, the surface tends to bend downward (Figure 4.6(B, D)). After the drilling stage, a local defect (bump) is created in the middle of the top surface due to drill torque (Figure 4.6(C, E)).

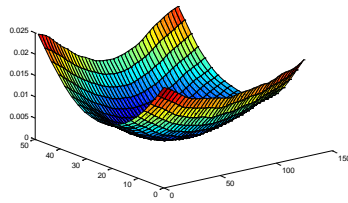


(A) Raw measurement data

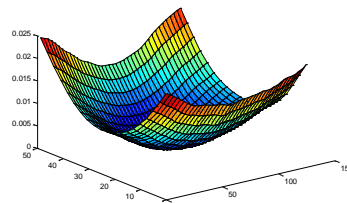


(B) After feature extraction

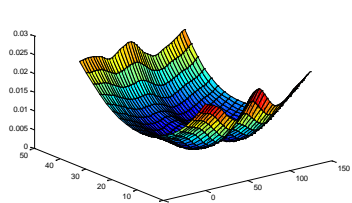
Figure 4.5 Feature extraction for global shape deformation



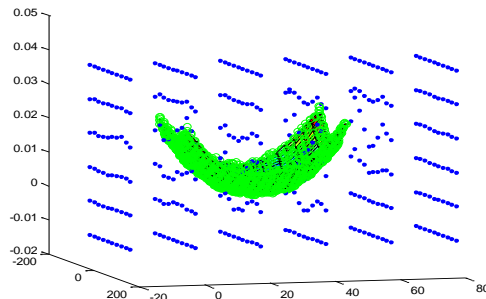
(A) Incoming surface



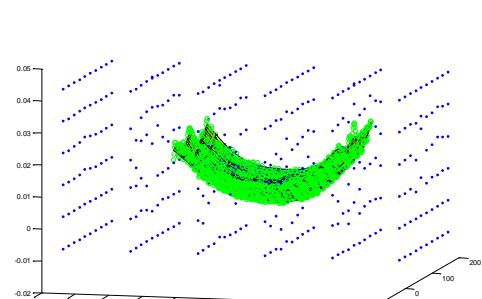
(B) Stage 1 surface



(C) Stage 2 surface



(D) Morphing prediction from initial stage to stage 1 (dots: lattice points of FFD volume, circles: surface of stage 1; surface: morphed surface of initial stage)



(E) Morphing prediction from stage 1 to stage 2 (dots: lattice points of FFD volume, circles: surface of stage 2; surface: morphed surface of stage 1)

Figure 4.6 Functional morphing for 2-stage manufacturing process

4.4.3. Inter-stage Process Adjustment

The simulation procedures of the two-stage process adjustment are given below:

- 1) Solve sensitivity matrix from variation sources to monitored surface grids by numerical methods (finite element analysis) at each stage;

- 2) Formulate the optimization problem defined in (4.18) and solve by iterative method;
- 3) Estimate the final surface flatness and variance.

A finite element model for each stage is developed using commercial software ABAQUS v6.8. In the face milling process (Figure 4.7), the initial surface is assumed to be flat with clamping force still applied right after the milling stage. After releasing the clamping force, deformation on the top surface is recorded. Four variation sources including fixtures and clamping forces have been identified and their distributions are listed in Table 4.4. Their sensitivity matrix for the face milling stage is then calculated.

Table 4.4 Variance sources in face milling stage

Variation Sources in Stage 1	Mean	Std. deviation
Fixture 1	0	2 μ
Fixture 2	0	2 μ
Clamping 1	20 MPa	2 MPa
Clamping 2	20 MPa	2 MPa

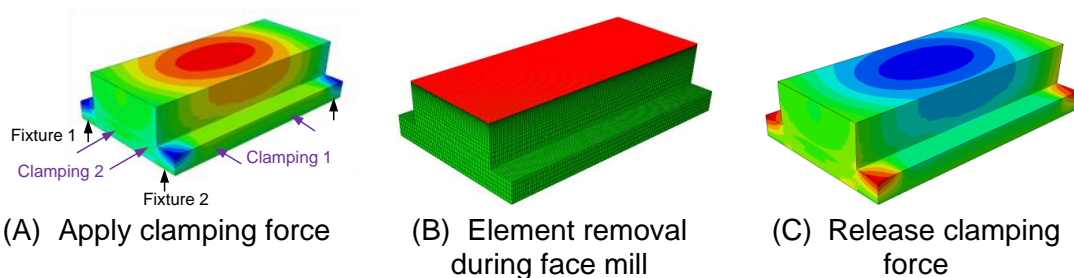


Figure 4.7 Finite element analysis of face milling process (displacement in Z)

The same procedure is conducted to simulate the sensitivity matrix for the drilling process (Figure 4.8) on 6 identified variation sources, whose distributions are listed in Table 4.5.

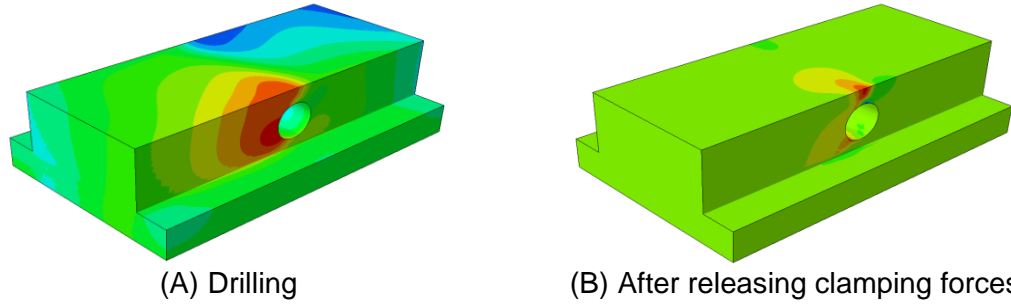


Figure 4.8 Finite element analysis of drilling process (displacement in Z)

Table 4.5 Variance sources in drilling stage

Variation Sources in Stage 2	Mean	Std. deviation
Fixture 1	0	2 μ
Fixture 2	0	2 μ
Clamping 1	20 MPa	2 MPa
Clamping 2	20 MPa	2 MPa
Drilling force	40 MPa	2 MPa
Thrust force	30 MPa	2 MPa

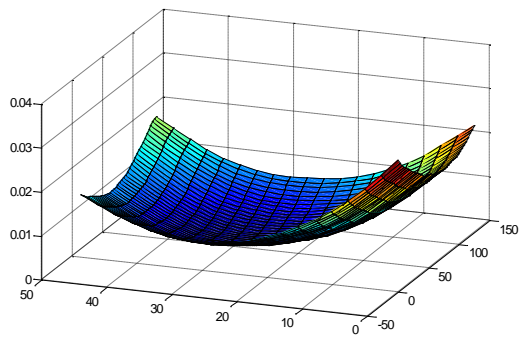
To simplify the presentation, only variation along Z direction is considered. Therefore, the Jacobian matrix in Eq. (4.14) becomes an 80×80 diagonal matrix. σ_{sp}^i and Σ_{sp}^i can be calculated by Eqs. (4.15)-(4.17).

Without losing generality, the incoming surface is assumed to be inclined with increased downward deformation in the middle as shown in Figure 4.9. Without adjustment, the final surface is inclined with a bump in the middle as shown in Figure 4.9(B) with solid color.

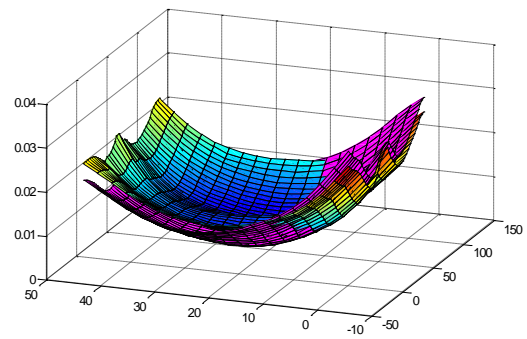
Table 4.6 Adjustable process parameters and optimal values

Variation Sources in Stage 1	Nominal	Range	Optimal Value	Variation Sources in Stage 2	Nominal	Range	Optimal Value
Fixture 1 (μ)	0	± 10	2.26	Fixture 1 (μ)	0	± 10	0.00
Fixture 2 (μ)	0	± 10	-5.58	Fixture 2 (μ)	0	± 10	0.00
Clamping 1 (MPa)	20	± 10	18.36	Clamping 1 (MPa)	20	± 10	20.51
Clamping 2 (MPa)	20	± 10	10.00	Clamping 2 (MPa)	20	± 10	17.65
				Drilling force (MPa)	40	± 10	38.13
				Thrust force (MPa)	30	± 10	32.83

Suppose the ranges of adjustable fixturing, clamping and process parameters are given in Table 4.6. After solving the optimization problem (4.18), the optimal solution is listed in columns 4 and 8 of Table 4.6. It is seen that in order to adjust the inclined incoming surface, during the face milling process, fixture 1 is moved upward while fixture 2 is moved downward, which produce the opposite of the original inclination . The clamping force 2 in stage 1 reduces to its minimum (10 MPa) and that in stage 2 continues to reduce by 2.35MPa in order to compensate the downward deformation in the middle of the part. Meanwhile, drilling force is reduced and thrust force is increased to improve the surface flatness. The final surface after adjustment is shown Figure 4.9(B) with blended color. It is seen that the final surface flatness and its variance are both improved, as listed in Table 4.7. Through inter-stage process adjustment, surface flatness in terms of height variance is reduced by 36% while the variance of flatness is reduced by 21.5%.



(A) Incoming surface



(B) Final surfaces with (blended color) and without (solid color) compensation

Figure 4.9 Case study on inter-stage form error compensation

Table 4.7 Comparison of surface flatness with and without compensation

	Without error-compensation	With error-compensation
Surface flatness	0.03431	0.02195
Sum of Variance	2.586×10^{-4}	2.030×10^{-4}

4.4.4. Backward Morphing Based Process Monitoring

This section demonstrates process monitoring through backward mapping and multivariate control chart. 100 parts are simulated using the optimized process parameters listed in Table 4.4 and Table 4.5 to estimate the between-part variation. Principal component analysis is performed on the surface data and a scree plot is shown in Figure 4.10. It is seen that the surface data are highly correlated since the first 3 principal components (PCs) capture over 99% of the total variation.

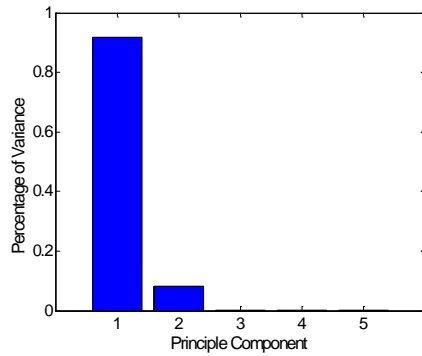


Figure 4.10 Scree plot of 100 training data

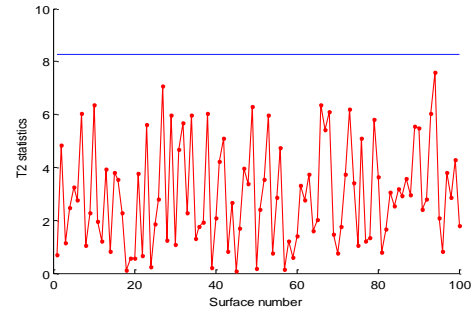
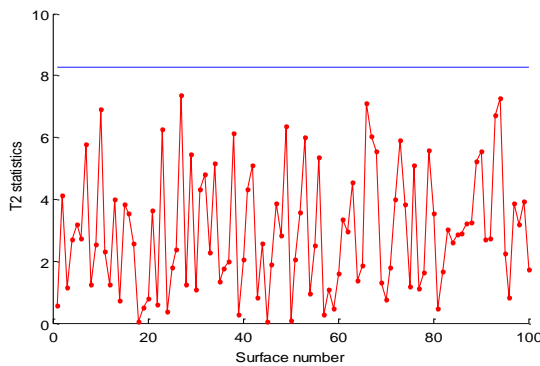
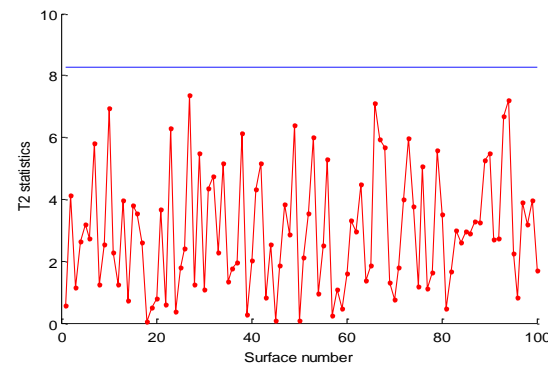


Figure 4.11 Phase I Hotelling's T^2 control chart at final stage

Assuming multivariate normality, Hotelling's T^2 control charts based on the 3 PC's are constructed to monitor the backward morphed surfaces at intermediate stages. The phase I control chart constructed by the 100 surfaces is shown in Figure 4.11. Figure 4.12 shows the control charts for stages 0 and 1. It should be noted that both control charts in Figure 4.12 are similar because clamping release at stage 1 has minor impact on surface change (Figure 4.6).



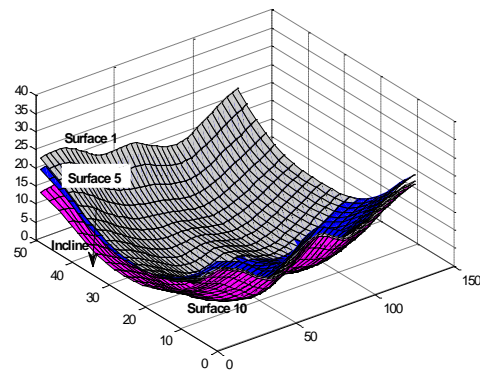
(A) Control chart of stage 1



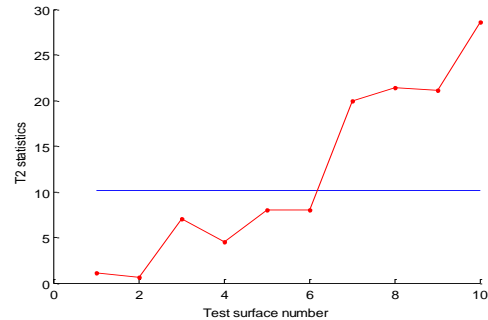
(B) Control chart of stage 0

Figure 4.12 Phase I Hotelling's T^2 control chart at prior stages

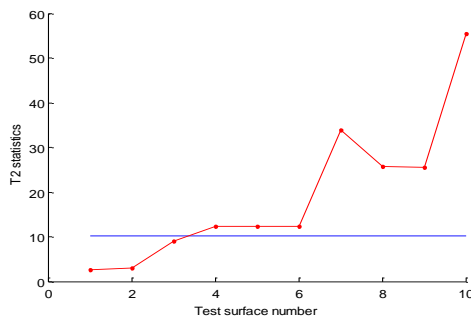
Phase II control chart is constructed to monitor 10 more surfaces that are manipulated by adding inclining trend to parts as shown in Figure 4.13 (A). In Figure 4.13(B-D) all three T^2 control charts shows out-of-control with linear trends.



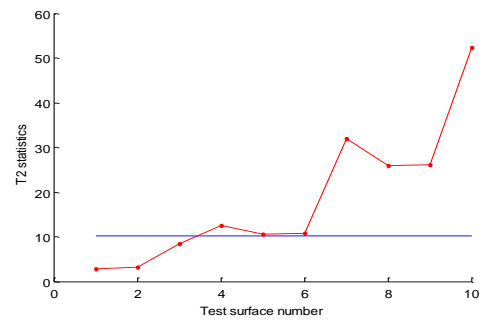
(A) New sample surfaces



(B) Control chart at stage 2



(C) Control chart at stage 1



(D) Control chart of stage 0

Figure 4.13 Phase II control charts

It is also interesting to observe that final stage under control doesn't require that all upstream stages are also under control. One example is surfaces #4-6 shown in Figure 4.13. This is because shape changes from different stages may cancel each other, which reduces mean-shift as detected by T^2 chart in the final stage. Therefore, in the case where final stage is under control while some previous stages are out-of-control, it is an indication of mean shift in the current process and further diagnosis is needed to detect the faulty stage.

4.5. CONCLUSION

This chapter conducts functional morphing modeling to obtain a better understanding of the part feature variation propagation and thereby improve the variation reduction strategy. A functional morphing based on FFD was developed and

represented by forward and backward mapping functions that capture feature changes as reflected from HDM data. Based on the established mapping functions, an inter-stage process adjustment method was developed to compensate for the form errors occurring at downstream stages. The repeatability of the adjustment strategy was ensured by a backward-morphing based monitoring scheme. The morphing functions in the adjustment algorithm need to be updated once an out-of-control signal indicates a process change. A case study based on a cutting experiment along with simulation demonstrated that the closed-loop adjustment strategy efficiently improved surface flatness.

Compared with the conventional research on variation propagation, the advantages of functional morphing for process control can be summarized as follows:

- *Improved geometry and texture characterization* The FFD based functional morphing can better describe the multi-scale feature changes (e.g., global shape, local deformation or waviness.) as well as their variations. Such changes can take place within each scale and potentially between scales. Thus, this approach will lead to a multi-scale variation propagation analysis that incorporates more variation sources for process control.
- *Incorporation of part physical properties* The impact of part physical properties on the surface feature change was considered via a bending energy term when deriving the mapping functions. It should be noted that the physical properties can be space-varying and time-varying. The functional morphing method therefore provides the opportunities of utilizing heterogeneous physical properties (e.g.,

distributions of mass density or casting pore density) for variation control in multistage precision machining.

- Improved characterization of form error cancellation The cancellation among complex form errors at different stages can be accurately acquired via morphing, which enables an inter-stage process monitoring and adjustment.
- High efficiency in dealing with HDM data The functional morphing methodology facilitates the HDM data analysis efficiently since it defines a FFD volume space on a sparse lattice and the volume space deforms between stages thereby avoiding dealing with dense HDM data directly. This approach will improve computational efficiency while satisfying both geometric constraint and physical feasibility.

REFERENCES

- Apley, D. and Shi, J., (2001), "A Factor-Analysis Method for Diagnosing Variability in Multivariate Manufacturing Processes", *Technometrics*, Vol. 43, pp. 84-95.
- Bookstein, F. L., (1989), "Principal Warps: Thin-Plate Splines and the Decomposition of Deformations", *IEEE Transactions on Pattern Analysis and Machine Intelligence*, Vol. 11, pp. 567-585.
- Cai, W., Hu, S.J. and Yuan, J., (1996), "A Variational Method of Robust Fixture Configuration Design for 3-D Workpiece", *ASME Transactions: Journal of Manufacturing Science and Engineering*, Vol. 119, pp. 593-602.
- Camelio, J., Hu, S.J. and Ceglarek, D., (2003), "Modeling Variation Propagation of Multi-Station Assembly Systems with Compliant Parts", *ASME Transactions: Journal of Mechanical Design*, Vol. 125, pp. 673-681.
- Coquillart, S., (1990), "Extended Free-form Deformation: A Sculpturing Tool for 3D Geometric Modeling", *ACM SIGGRAPH Computer Graphics*, Vol. 24, pp. 187-196.
- Ding, Y., Ceglarek, D. and Shi, J., (2002), "Fault Diagnosis of Multistage Manufacturing Processes by Using State Space Approach", *ASME Transactions: Journal of Manufacturing Science and Engineering*, Vol. 124 (2), pp. 313-322.

- Ding, Y., Jin, J., Ceglarek, D. and Shi, J., (2005), "Process-Oriented Tolerancing for Multi-Station Assembly Systems", *IIE Transactions*, Vol. 37, pp. 493-508.
- Djurdjanovic, D. and Ni, J., (2001), "Linear State Space Modeling of Dimensional Machining Errors", *Transactions of NAMRI/SME*, Vol. 29, pp.541-548.
- Hearn, D. and Baker, M.P., (1994), *Computer Graphics*, 2nd Edn., Prentice Hall, New York.
- Huang, Q. and Shi, J., (2003), "Simultaneous Tolerance Synthesis through Variation Propagation Modeling of Multistage Manufacturing Processes", *Transactions of NAMRI/SME*, Vol. 31, pp. 515-522.
- Huang, Q., Shi, J. and Yuan, J., (2003), "Part Dimensional Error and its Propagation Modeling in Multi-Stage Machining Processes", *ASME Transactions: Journal of Manufacturing Science and Engineering*, Vol. 125, pp. 255-262.
- Jin, J. and Shi, J., (1999), "State Space Modeling of Sheet Metal Assembly for Dimensional Control," *ASME Transactions: Journal of Manufacturing Science and Engineering*, Vol. 121, pp. 756-762.
- Keim, D. A. and Herrmann, A., (1998), "The Gridfit Algorithm: An Efficient and Effective Approach to Visualizing Large Amounts of Spatial Data", *IEEE Visualization: Proceedings of the Conference on Visualization*, pp. 181-188.
- Liu, J., Shi, J. and Hu, S.J., (2008) "Engineering-Driven Factor Analysis for Variation Sources Identification in Multistage Manufacturing Processes", *ASME Transactions: Journal of Manufacturing Science and Engineering*, Vol. 130, pp. 0410091-10.
- Mantripragada, R. and Whitney, D.E., (1999), "Modeling and Controlling Variation Propagation in Mechanical Assemblies Using State Transition Models", *IEEE Transactions on Robotics and Automation*, Vol. 15, pp. 124-140.
- Sederberg, T. W., and Parry, S. R., (1986), "Free-form Deformation of Polygonal Data", *Proceedings of International Electronic Image Week*, Nice, France pp. 633-639.
- Shi, J., (2006), "Stream of Variation Modeling and Analysis for Multistage Manufacturing Processes", CRC Press, Taylor & Francis Group.
- Taguchi, G., (1986), *Introduction to Quality Engineering*, Asian Productivity Organization, Tokyo, Japan.
- Ventsel, E. and Krauthammer, T., (2001), "Thin Plates and Shells: Theory, Analysis, and Applications", Marcel Dekker, New York.
- Wang, H. and Huang, Q., (2007), "Using Error Equivalence Concept to Automatically Adjust Discrete Manufacturing Processes for Dimensional Variation

Reduction", *ASME Transactions: Journal of Manufacturing Science and Engineering*, Vol. 129, pp. 644-652.

Wu, C. F. J. and Hamada, M., (2000), "Experiments: Planning, Analysis, and Parameter Design Optimization", John Wiley and Sons Inc, New York.

Zhong, J., Liu, J. and Shi, J., (2009), "Predictive Control Considering Model Uncertainty for Variation Reduction in Multistage Assembly Processes", *IEEE Transactions on Automation Science and Engineering*, Accepted as TASE-2009-091.

Zhou, S., Chen, Y. and Shi, J., (2004), "Statistical Estimation and Testing for Variation Root-Cause Identification of Multistage Manufacturing Processes", *IEEE transactions on Robotics and Automation*, Vol. 1, pp.73-83.

Zhou, S., Huang, Q. and Shi, J., (2003), "State Space Modeling for Dimensional Monitoring of Multistage Machining Process Using Differential Motion Vector", *IEEE Transactions on Robotics and Automation*, Vol. 19 (2), pp. 296-309.

CHAPTER 5

CONCLUSIONS AND FUTURE WORK

5.1. CONCLUSIONS

The research on functional morphing for manufacturing process design, evaluation and control originates from the rapidly changing market requirement to shorten product development time, as well as the constant need for manufacturing process monitoring and control. Since shape change is an important goal of most manufacturing processes, one potential solution facilitating process development is to describe the shape changes using morphing, which has been widely utilized in the areas of computer graphics, filming and medical imaging. However, current morphing techniques are geometry driven without considering physical feasibility. Hence there are limitations when these morphing techniques are used to characterize physical processes. Therefore, a *functional morphing* concept has been proposed by incorporating material and process considerations into geometric morphing. This dissertation is aimed to develop functional morphing algorithms for manufacturing process design and control. The developed methodologies enable an effective process design and evaluation for evolutionary product development through functional morphing between product generations. Meanwhile, these methodologies can also be

utilized for high-definition metrology based monitoring and control of multi-stage manufacturing systems.

The major achievements of this dissertation can be summarized in three parts:

- 1) *Development of a functional morphing methodology for stamping die face design of evolutionary products:* A new concept using functional morphing for evolutionary die development has been proposed using three sequential steps: part-to-part mapping between the existing part and the new part, die-to-die morphing using the same parts mapping function, and finite element verification. The mapping function is constructed by functional morphing combining both geometric relationship between part surfaces and a smoothness function which inherits the springback compensation information. Results show that the morphed new die can capture the difference of product design through generations as well as springback compensation from previous die design. This study is beneficial to die development of new product in the same product family or different generations utilizing the existing product and die information.
- 2) *Development of a functional morphing based strain increment method for formability assessment in die face morphing:* Based on the die face morphing algorithm, a strain increment method has been introduced to quickly predict the strain and evaluate the formability for a new part generation. This method calculates the strain increment associated with functional morphing between parts by introducing a bending energy and a strain gradient penalty term. By superposition of the strain increment to

the original strain from the existing part, the strain field on the new part can be estimated. Since this method does not require the knowledge on new die surface, such formability assessment can be used as an early feasibility assessment of the new part design.

- 3) *Investigation of functional morphing in process control for multi-stage manufacturing processes:* A functional morphing model is developed to investigate the part feature variation propagation for high-definition metrology data through a multi-stage manufacturing process and thereby improve the variation reduction strategy. This functional morphing incorporates heterogeneous material properties such as density distribution and is represented by forward and backward mapping functions. Based on the established mapping function, this study also develops an inter-stage process adjustment method to compensate for the form errors occurring at downstream stages. And the repeatability of the adjustment strategy is ensured by a backward-morphing based monitoring scheme.

The original contributions of this research can be summarized as follows:

- 1) A new concept of functional morphing is introduced by incorporating material and process information into the part geometry morphing. As such functional morphing can better describe the physical changes in manufacturing processes.
- 2) The concept of die face morphing is introduced to integrate the existing die information into new die design for evolutionary product development.

Guidelines are proposed by using functional morphing based part-to-part mapping, die-to-die morphing and finite element verification. It is found that the morphed new die is able to capture the springback compensation from the existing die by including a smoothness function in part-to-part mapping and thus reduce the design-engineering iteration.

- 3) A strain increment method is developed to quickly assess the formability of the new part using the geometric and strain information of its previous generation. Functional morphing including a bending energy and a strain gradient constraint is introduced to morph between part generations. It is found that the predicted strain distribution is well compared with that from finite element analysis.
- 4) The free-form deformation based functional morphing is developed to describe feature changes as well as their variations through multi-stage process. This approach can also lead to a multi-scale variation propagation analysis that incorporates more variation sources for process control. The cancellation among complex form errors at different stages is accurately acquired via morphing, which enables an inter-stage process monitoring and adjustment.
- 5) The functional morphing methodology is shown to improve computational efficiency while satisfying both geometric constraint and physical feasibility for the HDM data analysis.

5.2. FUTURE WORK

The methodologies and models proposed in this research could be further improved and /or extended in the following directions:

- 1) The die face morphing method can be further extended to other manufacturing processes designs for evolutionary products. For example, in machining process, tool path can be morphed from existing product to new product generation. In chemical mechanical polishing (CMP) process, wafer topography can be morphed from one product to another to quickly determine the process parameter adjustments.
- 2) The strain increment method can be improved by considering material flow and complex boundary conditions. In sheet metal stamping, the change of draw bead or blank holding force will affect material flows. The strain increment method can incorporate these changes by transforming them into equivalent constraints in functional morphing. Then, strain distribution under these complex boundary conditions and material flows can be estimated.
- 3) Formability estimation can be integrated into the die face morphing algorithm for better determination of the new generation stamping die. Formability is first estimated using the strain increment method combined with strain or stress based approaches. During die face morphing, the feasible solution region is further reduced by integrating the formability, resulting in a better die face considering both springback compensation and formability of the produced part.

- 4) The functional morphing modeling for multi-stage machining process can be extended to multi-scale morphing, where the impact of one scale (e.g., global shape) can be morphed from other scales (e.g., localized features) and vice versa. This can be done through morphing extrapolation from small scale to large scale, or multi-level morphing from large scale to small scale. Corresponding diagnosis and control strategies can be developed for multi-stage multi-scale process monitoring and control.
- 5) The morphing based process control for multi-stage processes can be extended to other manufacturing processes, such as multi-stage stamping process including blanking, stamping, re-strikes, trimming, flanging and hemming. Sheet metal products in the multi-stage stamping process can be morphed through each operation. The developed inter-stage form error compensation and monitoring methodologies can be utilized to adjust these operations to compensate springback and reduce final product variability.